Published in final edited form as:
J Comp Neurol. 2011 August 15; 519(12): . doi:10.1002/cne.22657.

Cytoarchitecture and Ultrastructure of Neural Stem Cell Niches and Neurogenic Complexes Maintaining Adult Neurogenesis in the Olfactory Midbrain of Spiny Lobsters, *Panulirus argus*

Manfred Schmidt[*] and **Charles D. Derby**
Neuroscience Institute and Department of Biology, Georgia State University, Atlanta, Georgia 30303

Abstract

New interneurons are continuously generated in small proliferation zones within neuronal somata clusters in the olfactory deutocerebrum of adult decapod crustaceans. Each proliferation zone is connected to a clump of cells containing one neural stem cell (i.e., adult neuroblast), thus forming a "neurogenic complex." Here we provide a detailed analysis of the cytoarchitecture of neurogenic complexes in adult spiny lobsters, *Panulirus argus*, based on transmission electron microscopy and labeling with cell-type-selective markers. The clump of cells is composed of unique bipolar clump-forming cells that collectively completely envelop the adult neuroblast and are themselves ensheathed by a layer of processes of multipolar cell body glia. An arteriole is attached to the clump of cells, but dye perfusion experiments show that hemolymph has no access to the interior of the clump of cells. Thus, the clump of cells fulfills morphological criteria of a protective stem cell niche, with clump-forming cells constituting the adult neuroblast's microenvironment together with the cell body glia processes separating it from other tissue components. Bromodeoxyuridine pulse-chase experiments with short survival times suggest that adult neuroblasts are not quiescent but rather cycle actively during daytime. We propose a cell lineage model in which an asymmetrically dividing adult neuroblast repopulates the pool of neuronal progenitor cells in the associated proliferation zone. In conclusion, as in mammalian brains, adult neurogenesis in crustacean brains is fueled by neural stem cells that are maintained by stem cell niches that preserve elements of the embryonic microenvironment and contain glial and vascular elements.

INDEXING TERMS

proliferation; decapod crustacean; arthropod; brain; glia

Neurogenesis persists throughout adulthood and leads to continuous production of new neurons in certain brain regions. Adult neurogenesis is well documented in brains of mammals and other vertebrates, including fish, amphibians, reptiles, and birds, but it is also a constitutive process in brains of many arthropods (Lindsey and Tropepe, 2006). In mammalian brains, adult neurogenesis predominantly produces new local interneurons of the olfactory bulb (periglomerular cells and granule cells) and the hippocampal dentate gyrus (granule cells; Kriegstein and Alvarez-Buylla, 2009). In brains of some insect species, adult neurogenesis generates new local interneurons (Kenyon cells) of the mushroom bodies (Cayre et al., 1994, 1996; Gu et al., 1999; Dufour and Gadenne, 2006; Mashaly et al., 2008; Zhao et al., 2008; Ghosal et al., 2009). The mushroom bodies are large protocerebral

[*]CORRESPONDENCE TO: Manfred Schmidt, Neuroscience Institute, Georgia State University, P.O. Box 5030, Atlanta, GA 30302-5030. mschmidt@gsu.edu.

neuropils that in most insects receive projections neurons (PNs) from the antennal lobes and thus represent the second stage of the central olfactory pathway; moreover, they are centers for multisensory integration (Strausfeld et al., 2009). Throughout decapod crustaceans, adult neurogenesis leads to the formation of new local interneurons (LNs) and projection neurons (PNs) of the olfactory deutocerebrum (midbrain), representing the first stage of the central olfactory pathway (Schmidt, 1997, 2001, 2007a; Sandeman et al., 1998, 2009; Harzsch et al., 1999; Schmidt and Harzsch 1999; Hansen and Schmidt, 2001, 2004; Sullivan and Beltz, 2005a, b; Sullivan et al., 2007a; Song et al., 2009; Zhang et al., 2009). Constitutive components of the decapod crustaceans' olfactory deutocerebrum are the bilaterally paired olfactory lobe (OL), a large neuropil organized into wedge-shaped glomeruli receiving afferent input from olfactory receptor neurons, and two bilaterally paired clusters of neuronal somata, medial cluster (MC) containing the somata of local interneurons (LNs) and the lateral cluster (LC) containing the somata of PNs (see Fig. 1; Sandeman et al., 1992; Schachtner et al., 2005). In Achelata (spiny and slipper lobsters) and Astacidea (clawed lobsters and crayfish), an additional large, bilaterally paired neuropil, the accessory lobe (AL), is present in the olfactory deuto-cerebrum. In these taxa, the deutocerebral PNs are differentiated into OL-specific and AL-specific ones, and both types develop a thin axon ascending within a common fiber tract (olfactory glomerular tract) to the lateral protocerebrum (Wachowiak and Ache, 1994; Wachowiak et al., 1996; Schmidt and Ache, 1996; Sullivan and Beltz, 2001).

The occurrence of adult neurogenesis in two distinct animal phyla, vertebrates and arthropods, poses two overarching questions. 1) Is adult neurogenesis based on the same or different types of neural stem cells (NSCs) and cell lineages as embryonic neurogenesis? 2) Are there common cellular mechanisms ensuring the lifelong maintenance of mitotically active NSCs in specific brain areas? In Bilateria, the central nervous system is of ectodermal origin, and, in vertebrates as well as in Tetraconata (=Pancrustacea, the likely monophyletic taxon comprising insects and crustaceans established through modern phylogenetic analyses; Dohle, 2001; Telford et al., 2008; Regier et al., 2010), embryonic neurogenesis begins with the differentiation of NSCs from neuroepithelial cells (Egger et al., 2008; Ungerer and Scholtz, 2008; Kriegstein and Alvarez-Buylla, 2009). However, embryonic NSCs and the cell lineages they generate differ fundamentally between vertebrates and Tetraconata. In vertebrates, the NSCs fueling embryonic neurogenesis are radial glial cells, which are ciliated and have a distinct bipolar morphology. Radial glial cells undergo serial asymmetric cell divisions in which they self-renew and produce a daughter that is either an immature neuron or an intermediate progenitor cell (Alvarez-Buylla et al., 1998; Kriegstein and Alvarez-Buylla, 2009). Adult neurogenesis in mammalian brains is maintained by NSCs that have the morphology of mature astrocytes, are endowed with a primary cilium, and are derived from radial glial cells. These "astrocytic" NSCs are scattered throughout extensive germinal layers: the subventricular zone lining the lateral ventricles and the subgranular zone of the dentate gyrus. They are largely quiescent (retaining labeled DNA for long periods of time), and they give rise to transit-amplifying intermediate progenitor cells that divide rapidly (Doetsch et al., 1999a,b; Palmer, 2000; Alvarez-Buylla et al., 2001; Merkle et al., 2004; Breunig et al., 2008; Han et al., 2008; Mirzahdeh et al., 2008; Kriegstein and Alvarez-Buylla, 2009).

In Tetraconata, the NSCs maintaining embryonic neurogenesis are large globular neuroblasts (NBs) that have no bipolar or otherwise glial morphology and are not ciliated. Through serial asymmetrical divisions, NBs self-renew and produce smaller daughter cells called *ganglion mother cells* (GMCs) toward the inside of the body. GMCs undergo a terminal symmetrical division in which two immature neurons are produced. Typically GMCs and immature neurons produced by one NB stay attached to it, forming a column or small aggregate of cells (Dohle, 1976; Doe and Goodman, 1985; Hartenstein et al., 1987;

Scholtz, 1992; Doe et al., 1998; Harzsch, 2001; Urbach and Technau, 2003; Egger et al., 2008; Ungerer and Scholtz, 2008; Boyan et al., 2010). In insects, some embryonic NBs become quiescent and are reactivated during larval stages to fuel larval neurogenesis in most parts of the CNS (Maurange and Gould, 2005), except for the optic lobes, where new NBs are generated from neuroepithelial cells (Yasugi et al., 2008). Most larval NBs of insects give rise to immature neurons by the same cell lineage as embryonic NBs (Bello et al., 2008). Recently, it was discovered that some embryonic and larval NBs of the insect brain proliferate in a more complex way and give rise to larger lineages. These NBs produce intermediate progenitor cells that act as self-renewing transit-amplifying cells that give rise to GMCs (Bello et al., 2008; Boone and Doe, 2008; Bowman et al., 2008; Izergina et al., 2009; Boyan et al., 2010). Adult neurogenesis in the mushroom bodies of insects is based on continued mitotic activity of a few NBs surviving after larval development (Cayre et al., 1994, 1996, 2002; Gu et al., 1999; Dufour and Gadenne, 2006; Mashaly et al., 2008; Zhao et al., 2008; Ghosal et al., 2009). These adult NBs appear to generate progeny as the canonical embryonic and larval NBs (Dufour and Gadenne, 2006; Zhao et al., 2008); however, the exact cell lineage that they produce has not yet been established.

In the olfactory deutocerebrum of adult decapod crustaceans, new neurons arise in small proliferation zones of invariant location at the inner (neuropil-facing) surface of the neuronal soma clusters (MC, LC). The proliferating cells in these zones are small and equivalent to GMCs in giving rise to immature neurons through one round of symmetrical cell divisions. Neuronal differentiation of these cells takes months and is associated with their translocation away form the proliferation zone into the outer area of the respective soma cluster (Fig. 1; Schmidt, 2001; Sullivan and Beltz, 2005a). Recently, it was determined that, in adult spiny lobsters, *Panulirus argus*, and crayfish, *Procambarus clarkii*, each proliferation zone is associated with a particularly large proliferating cell that has an invariant location outside the proliferation zone but is connected to it via a strand- or duct-like structure (Schmidt, 2007a; Song et al., 2009). Based on their large size and privileged location, these cells were identified as putative adult neuroblasts (aNBs). Thus, adult neurogenesis in the olfactory deutocerebrum of decapod crustaceans appears to be maintained by NSCs and neural progenitor cells that are equivalent to those fueling embryonic neurogenesis, NBs and GMCs, respectively.

A common theme in the de novo generation of cells in various tissues of adult animals is that the new cells are produced by adult (somatic) stem cells residing in specialized microenvironments within the tissues. These areas represent stem cell niches, providing regulatory input and nutritional support for the adult stem cells and possibly shielding them from toxic or harmful factors (Spradling et al., 2001; Fuchs et al., 2004; Ohlstein et al., 2004; Moore and Lemischka, 2006; Jones and Wagers, 2008; Morrison and Spradling, 2008). The NSCs in brains of adult mammals reside in stem cell niches that form a distributed and complex structural meshwork pervading the germinal cell layers. These NSC niches are composed of vascular elements, glial cells, and extracellular matrix (Palmer et al., 2000; Mercier et al., 2002; Shen et al., 2008; Tavazoie et al., 2008). In the olfactory deutocerebrum of adult *P. argus* and *P. clarkii*, each aNB is closely associated with a morphologically unique clump of cells that has been interpreted as a putative stem cell niche (Fig. 1; Schmidt, 2007a,b; Sullivan et al., 2007a,b; Song et al., 2009). Similar clumps of cells were originally identified as “deutocerebral organs” in brains of several other species of decapod crustaceans by Bazin (1970) suggesting that they are a common component associated with adult neurogenesis in the olfactory deutocerebrum (Schmidt, 2007b). The clump of cells containing the aNB, the proliferation zone associated with it, and the duct- or strand-like structure connecting both compartments form a structural unit for which we use the term *neurogenic complex*, as previously established (Song et al., 2009).

Here we provide a detailed analysis of the cytoarchitecture of the neurogenic complexes in olfactory deutocerebrum of adult spiny lobsters, *P. argus*, based on transmission electron microscopy and labeling with cell-type-selective markers. This study provides the foundation for an in-depth analysis of the cellular interactions between aNBs and their niche, utilizing the unique advantage that they form morphologically identifiable units in the brain of adult decapod crustaceans.

MATERIALS AND METHODS

Animals

Experiments were performed on intermolt male and female Caribbean spiny lobsters, *Panulirus argus*, ranging from 50 to 80 mm in carapace length and from 120 to 400 g in weight. Since female *P. argus* reach sexual maturity (as indicated by spawning resulting in the presence of eggs attached to the pleopods) at a minimum size of 52 mm carapace length (Lyons et al., 1981), the experimental animals likely comprised mostly adults and some late juveniles. Most animals were obtained from the Florida Keys Marine Laboratory, shipped to Georgia State University, and held in communal 800-L aquaria containing aerated, recirculated, filtered artificial seawater (ASW; Instant Ocean: Aquarium Systems, Mentor, OH). Animals were maintained in a 12-hour:12-hour light:dark cycle and fed shrimp or squid three times per week. Some animals were kindly provided by Dr. B. W. Ache (University of Florida) and were kept under similar conditions. Animals were anesthetized by chilling on ice for at least 15 minutes before removal of brains or establishing excised head preparations.

Chemicals

All chemicals were obtained from Sigma (St. Louis, MO) unless specified otherwise.

Transmission electron microscopy

For analysis of the ultrastructure of the neurogenic complex in the LC of *P. argus*, three brains were perfusion fixed with 5% glutaraldehyde in 0.1 M Sörensen phosphate buffer (SPB) containing 15% sucrose (SPBS) via the cannulated cerebral (medial) artery in an excised head preparation as described in detail previously (Schmidt and Ache, 1994). Brains were removed from the head and immersed in fixative for another 4 hours at room temperature, rinsed in SPBS for 4 × 30 minutes, postfixed in 2% OsO_4 in SPBS for 2 hours, rinsed in SPBS for 4 × 30 minutes, dehydrated in an ascending ethanol series, incubated in propylene oxide for 2 × 30 minutes, and embedded in Epon 812 hard with polymerization at 60°C for 18 hours. Serial ultrathin sections (90–100 nm thick) were cut with a diamond knife (Diatome AG, Biel, Switzerland) on an ultramicrotome (Ultracut; Reichert-Jung, Vienna, Austria), contrasted for 20 minutes with lead citrate, and examined in a transmission electron microscope (LEO 906e; LEO Elektronenmikroskopie, Oberkochen, Germany). Images were acquired digitally with an attached CCD camera with 1 MP resolution. The digital images were processed by filtering out high-frequency noise and by adjustment of brightness and contrast with an image analysis program (Image Pro Express, version 4.5.1.3; Media Cybernetics, Bethesda, MD) before they were arranged into the final figures with an illustration program (Illustrator CS3; Adobe, San Jose, CA).

Data analysis

In TEM micrographs, the size and shape of different cell types and their nuclei were determined by tracing cell membrane and nucleus with an image analysis program (Image Pro Express). From the length of the outline (perimeter) and the included area, two parameters representing size and shape of the measured structures were calculated: size is

given as Feret diameter (FD; diameter of a circle having the same area as the measured area: FD = sqrt [4 × area/π]); shape is given as roundness (R; a dimensionless number between 0 and 1 with 1 representing a perfect circle: R = [4 × π × area)/perimeter^2]). For cell types in which the size of the soma and the size of the nucleus could be determined, the nuclear:cytoplasmic ratio was calculated by division of the nuclear volume (derived from the nuclear Feret diameter, assuming a spherical shape) by the volume of the cytoplasm (derived by subtracting the nuclear volume from the soma volume, which was derived from the soma Feret diameter, assuming a spherical shape). The results of the measurements are given as arithmetic mean ± standard deviation. Two data analysis programs were used to treat the data statistically and to generate graphs (PsiPlot 7.01; Poly Software International, Pearl River, NY; and GraphPad Prism 3.02; GraphPad Software, San Diego, CA). The final figures containing these graphs were created with an illustration program (Illustrator CS3).

Fluorescence microscopy

BrdU injection—For in vivo labeling, 5-bromo-2′-deoxyuridine (BrdU) was injected at the base of two walking legs into the hemolymph of 18 spiny lobsters at 5 mg BrdU/100 g body weight (0.5% BrdU in *Panulirus* saline: 459 mM NaCl, 13.4 mM KCl, 13.6 mM $CaCl_2$, 14.1 mM Na_2SO_4, 9.8 mM $MgCl_2$, 3.0 mM Hepes, pH 7.4). All animals received one BrdU injection between 8:00 and 10:00 AM, and after a survival time of 2–10 hours their brains were dissected and fixed for 24 hours at room temperature by immersion in 4% paraformaldehyde in SPBS (PFA).

Perfusion of brain arteries with fluorescent dextran—In an excised head preparation of *P. argus*, the cerebral artery was cannulated and the brain perfused with *Panulirus* saline at a flow rate of 1 ml/min as described in detail earlier (Schmidt and Ache, 1994). After 15 minutes of saline perfusion, 1 ml *Panulirus* saline containing 1 mg/ml dextran coupled to lysine-fixable tetramethylrhodamine (3,000 MW microruby for two brains; 10,000-MW miniruby for two brains; Invitrogen/Molecular Probes, Carlsbad, CA) was perfused over 5 minutes into the cerebral artery. After 5 minutes of incubation without perfusion, the brain was fixed by immersion in PFA for 24 hours at room temperature.

Sectioning and immunocytochemistry

In addition to brains preloaded with BrdU or fluorescent dextran, >100 brains were fixed by immersion in PFA for 24 hours at room temperature to be used for immunocytochemical labeling with other antibodies or fluorescent lectins. After fixation, brains were rinsed and stored in 0.02 M SPB with 0.02% sodium azide at 4°C. For sectioning, brains were embedded in gelatin and cut on a vibrating microtome (VT 1000 S; Leica, Wetzlar, Germany) in 80-μm-thick horizontal or sagittal sections as described in detail previously (Schmidt, 2001). All of the following treatments were performed at room temperature.

Most brains preloaded with BrdU were triple labeled with anti-BrdU (labeling cells that were in S-phase when BrdU was available for incorporation into newly synthesized DNA), antiphosphohistone H3 (Ser 10; anti-pH3; labeling cells that were in M-phase at the time of fixation), and the nuclear marker Hoechst 33258 (labeling nuclei of all cells). To overcome the common problem that the pre-treatment of sections required for intense BrdU labeling severely compromises general nuclear staining (Tang et al., 2007), we developed a protocol based on the mild digestion of double-stranded DNA with DNase I (Ye et al., 2007). In this optimized triple-labeling protocol, free-floating sections were first incubated in 2 N HCl for 20 minutes and rinsed for 4 × 10 minutes in SPB. Afterward, sections were incubated overnight in anti-BrdU (mouse monoclonal, clone B44; BD Biosciences, Franklin Lakes, NJ; Table 1) diluted 1:150 in a DNase-containing incubation medium. This medium consisted of a 1:1 mixture of SPB with 0.3% Triton X-100 (TSPB) and DNase I buffer (50

mM Tris HCl at pH 7.5, 5 mM $MgCl_2$, 50 μg/ml bovine serum albumin, and 0.3% Triton X-100) to which 10 U DNase I/ml and 10 μg/ml of a protease inhibitor cocktail (Sigma P-2724) were added. Subsequently, sections were rinsed for 4 × 30 minutes in TSPB and incubated overnight in anti-pH3 (rabbit polyclonal, No. 06-570; Upstate Biotechnology, Lake Placid, NY; Table 1) at 1:250 dilution in TSPB to label cells in M-phase. After the sections had been rinsed for 4 × 30 minutes in TSPB, they were incubated in a mixture of two secondary antibodies: goat anti-mouse Cy3 (Jackson Immunoresearch, West Grove, PA) diluted 1:400 and goat anti-rabbit AlexaFluor-488 (Invitrogen/Molecular Probes) or goat anti-rabbit DyLight-488 (Jackson Immunoresearch) diluted 1:100 in TSPB. After rinsing for 3 × 30 minutes in SPB, sections were incubated for 20 minutes in Hoechst 33258 diluted 1:150 in SPB from a stock solution of 1 mg/ml to stain nuclei. After a final rinse in SPB, sections were coverslipped in 1:1 glycerol:SPB containing 5% diaza-bicyclol[2.2.2]octane (DABCO) to prevent photobleaching. Coverslips were secured with nail polish, and slides were stored at 4°C or at −20°C (for extended periods).

Brains in which the arterial system was perfused with fluorescent dextran were sectioned as described above. Sections were only incubated in Hoechst 33258 and then coverslipped.

In an effort to identify selective markers for particular cell types or other structures in the brain of *P. argus*, we screened >120 antibodies and >30 lectins by labeling brain sections that were generated as described above. Each antibody and lectin was tested on sections of at least two brains containing the neurogenic complex of MC or LC, with TSPB serving as antibody incubation medium. Here, we include only those probes that are of interest for this study, and the results of the entire screen will be described in detail elsewhere. We report results obtained with the following four antibodies (Table 1) and four lectins: antisynapsin (anti-Syn; mouse monoclonal from Developmental Systems Hybridoma Bank; 3C11) diluted 1:25; antiglutamine synthetase (anti-GS; mouse monoclonal from BD Biosciences; No. 610518) diluted 1:100; anti-Gαs/olf (anti-Gs/olf; rabbit polyclonal from Santa Cruz Biotechnology, Santa Cruz, CA; SC-383) diluted 1:200; anti-spiny lobster achaete scute homolog (anti-Splash; rabbit polyclonal antiserum raised by Dr. Hsin Chien against the polypeptide sequence from aa 133–265 of *splash* expressed in *Escherichia coli*; Chien et al., 2009; GenBank accession No. DQ489559) diluted 1:400; wheat germ agglutinin (WGA) labeled with Alexa-Fluor-488 (Molecular Probes/Invitrogen) diluted 1:1,000; *Amaranthus caudatus* lectin (ACL) labeled with fluorescein isothiocyanate (Vector, Burlingame, CA) diluted 1:1,000; *Helix pomatia* agglutinin (HPA) labeled with Alex-aFluor-488 (Molecular Probes/Invitrogen) diluted 1:200; and soy bean agglutinin (SBA) labeled with fluorescein isothiocyanate (Vector) diluted 1:200. The primary antibodies were visualized by incubating the sections with Cy3-labeled secondary antibodies (goat anti-rabbit for anti-Gs/olf and anti-Splash, goat anti-mouse for anti-Syn and anti-GS; Jackson Immunoresearch) diluted 1:400 in TSPB for at least 4 hours at room temperature. To obtain sections double labeled with an antibody and a lectin, the lectin was added to the medium containing the secondary antibody. Finally, all sections were labeled with Hoechst 33258 and coverslipped as described above. In the case of anti-GS, positive labeling was achieved only in brain sections that had been incubated for 20 minutes in 2 N HCl (as required for labeling with anti-BrdU) prior to incubation in the primary antibody.

In controls, sections from brains of two spiny lobsters that had received no BrdU injection were treated as for labeling with anti-BrdU and anti-pH3 but without including the primary anti-pH3 antibody in the incubation medium. In these sections, no specific labeling above the autofluorescence of the tissue was observed.

Antibody and lectin characterization: Western blot analysis

Except for anti-BrdU and anti-pH3 that we employed to identify cells in S-phase (at the time of BrdU availability) and M-phase (at the time of fixation) of the cell cycle, respectively, the other antibodies and lectins included in this study were used as purely morphological markers, allowing selective labeling of cell types or tissue components and thereby distinguishing them from each other. We do not make any functional inferences based on the labeling with these probes and therefore did not strive rigorously to establish the molecular identity of the antigens or binding sites responsible for probe binding. To test the specificity of anti-Gs/olf, anti-GS, and anti-Splash, we performed Western blot analyses with these three antibodies on *P. argus* brain extracts based on a detailed protocol published previously (Schmidt, 2007a).

Anti-BrdU—Diverse antibodies against BrdU were used previously in decapod crustacean brains to label cells in S-phase (see references cited in the introductory paragraphs). The monoclonal mouse anti-BrdU that we used in this study (clone B44; BD Biosciences) was raised against a 5-iodo-2′-deoxyuridine conjugated to ovalbumin and binds to 5-bromo-2′-deoxyuridine as well as 5-iodo-2′-deoxyuridine according to the manufacturer's information. The staining pattern obtained with this antibody was indistinguishable from that obtained with other BrdU antibodies in previous studies (Schmidt, 2001, 2007a). Because no labeling was present in brains of animals that had not received a BrdU injection, we conclude that labeling with anti-BrdU specifically labeled nuclei that incorporated BrdU into newly synthesized DNA and thus were in the S-phase of their cell cycle when BrdU was available.

Anti-pH3—The rabbit polyclonal antibody against phosphohistone H3 (Ser 10; No. 06-570; Upstate Biotechnology) was raised against the synthetic peptide ARK[pS]TGG-KAPRKQLC coupled to keyhole limpet hemocyanin according to the manufacturer's information. As in a previous study (Schmidt, 2007a), we found that it intensely labels select nuclei in the neurogenic complexes (and very occasionally in other locations) that have morphological features (condensation, irregular shape, pairwise apposition) of nuclei in various phases of mitosis. Since Western blot analysis of *P. argus* brain extracts provided evidence for the binding of this antibody to two isoforms of authentic phosphohistone H3 (Ser 10; Schmidt, 2007a), which are present only in the M-phase of the cell cycle (Hendzel et al., 1997; Wei et al., 1998), we conclude that the nuclear labeling of anti-pH3 is specific for M-phase nuclei. However, as in a previous study (Schmidt, 2007a), we found additional labeling of fibrous material surrounding the clump of cells and the duct extending from it to the adjacent proliferation zone. Based on two lines of evidence, we conclude that the labeling of this material is likely based on nonspecific binding of anti-pH3. First, a new batch of this antibody as well as several other anti-pH3 antibodies that we tested labeled select nuclei in the neurogenic complexes but not the fibrous material. Second, a previous Western blot analysis of *P. argus* brain extracts provided evidence for the nonspecific binding of this antibody to nonnuclear proteins of much higher molecular weights than typical for histones (Schmidt, 2007a).

Anti-Syn—The antibody against the synaptic protein synapsin was a mouse monoclonal antibody raised against the small isoform of synapsin (SYNAORF-1) from *Drosophila*. This antibody that we obtained from the Developmental Studies Hybridoma Bank was originally developed by Dr. Erich Buchner (Klagges et al., 1996). In Western blot analyses of *Drosophila* brains, anti-syn labeled prominent protein bands at 70, 74, and 80 kDa and a less prominent double band at ~143 kDa, indicating that four or five synapsin isoforms are detected (Klagges et al., 1996). In Western blot analyses of brain extracts of *Coenobita clypeatus* (terrestrial hermit crab), anti-syn labeled a prominent protein band at 80–90 kDa and a weaker protein band slightly above 148 kDa, indicating that two synapsin isoforms

corresponding to some of the isoforms present in *Drosophila* are detected (Klagges et al., 1996; Harzsch and Hansson, 2008). Anti-syn has been shown repeatedly to label selectively neuropil areas in the CNS of diverse decapod crustaceans (Harzsch et al., 1997, 1998, 1999; Sullivan et al., 2007a; Harzsch and Hansson, 2008), and we use it here to distinguish neuropils from other tissue components (especially neuronal soma clusters) in the brain of *P. argus*.

Anti-Gs/olf—The antibody against the heterotrimeric G-protein subunit Gαs/olf (C-18; Santa Cruz Biotechnology; sc-383) was an affinity-purified rabbit polyclonal antibody raised against aa 377–394 of Gαs of rat origin, mapping at the carboxy terminus (according to information provided by the manufacturer). In the clawed lobster *Homarus americanus*, Gαs was identified through molecular cloning and Western blot analysis of brain extracts with the same antibody as used here and showed a single band of 51.8 kDa (Xu et al., 1997). Our Western blot analysis of *P. argus* brain extracts with anti-Gs/olf diluted 1:1,000 revealed double bands at slightly higher molecular mass (~61/63 kDa) and in addition a strongly stained band at about twice this molecular mass (~137 kDa; Fig. 2A). Although the bands at ~61/63 kDa could be consistent with binding of the antibody to authentic Gαs given the tendency of G protein subunits to run anomalously high in SDS-PAGE gels (Quan and Forte, 1990; Xu et al., 1997), the strong band at ~137 kDa indicates nonspecific binding of the antibody to an unrelated protein of higher molecular mass.

Anti-GS—The monoclonal mouse antibody against glutamine synthetase (No. 610518; BD Biosciences) was raised against sheep glutamine synthetase (aa 1–373) according to the manufacturer's information. A crustacean glutamine synthetase was identified through molecular cloning in *P. argus* (Trapido-Rosenthal et al., 1993), and an affinity-purified rabbit polyclonal antibody raised against glutamine synthetase from chicken retina was used in *P. argus* for Western blot analyses of brain extracts and an immunocytochemical analysis of brain sections (Linser et al., 1997). The Western blots revealed a protein band at 42 kDa consistent with the expected size of *P. argus* glutamine synthetase as predicted from the cDNA, and the immunocytochemical analysis showed selective labeling of a particular type of glia with somata located at the rim of neuropils and processes reaching into the neuropils' interior. From these findings, Linser et al. (1997) concluded that glutamine synthetase is expressed in a particular type of glial cell and that anti-GS can serve as a glia-specific marker. Since the affinity-purified antibody used by Linser et al. (1997) is no longer available and the raw GS antiserum (kindly provided by Dr. Paul Linser, Whitney Laboratory, University of Florida) did not selectively label glial cells in *P. argus* brains in preliminary trials (Schmidt, unpublished), we used another antibody against vertebrate GS. The choice of anti-GS (No. 610518; BD Biosciences) was based on previous studies in other decapod crustaceans in which this antibody selectively labeled similar glial cells in the brain as described for *P. argus* (Sullivan and Beltz, 2005b; Sullivan et al., 2007a; Harzsch and Hansson, 2008). Our Western blots of *P. argus* brain extracts with anti-GS diluted 1:2,000 showed one band at ~42 kDa consistent with the previous report by Linser et al. (1997) and with the interpretation that it represents authentic *P. argus* GS (Fig. 2B). However, our Western blots show a second and more intensely labeled band at ~120 kDa that corresponds neither to the size of a GS subunit (at ~42 kDa) nor to the predicted size of the functional protein consisting of eight or 10 identical subunits (Eisenberg et al., 2000; Krajewski et al., 2008). An intense band of similar size was obtained in Western blots of crayfish nerve extracts probed with a different antibody against GS (McKinnon et al., 1995). The intense labeling of an additional protein band with anti-GS as seen in our Western blot analyses makes it likely that on tissue sections anti-GS also labels this unrelated protein in addition to labeling authentic glutamine synthetase. Thus, some of the cellular labeling achieved with anti-GS may be nonspecific.

Anti-Splash—In the context of an unrelated project aimed at the molecular identification of transcription factors involved in crustacean adult neurogenesis, we identified a spiny lobster achaete scute homolog (Splash) by molecular cloning (Chien et al., 2009). We attempted to raise polyclonal antibodies against Splash protein by immunizing 10 rabbits with different segments of the protein that were heterologously expressed in *E. coli*. We tested the suitability of all antibodies for immunocytochemistry by labeling sections of diverse *P. argus* tissues, including brain. One antibody (anti-Splash5-5; rabbit No. 5, fifth bleed) that was raised against a large portion of the Splash protein that included a part of the conserved basic helix–loop–helix domain but not the C-terminal domain (AA 133–265) resulted in highly selective labeling of a structure within the neurogenic complexes of the brain, and results obtained with this antibody are reported here. Western blot analysis of *P. argus* brain extracts with anti-Splash5-5 (Fig. 2C) revealed labeling of at least six prominent protein bands, none of which had the predicted molecular mass of *P. argus* Splash (~30 kDa; Chien et al., 2009). Thus we conclude that the staining of brain sections obtained with anti-Splash5-5 does not reflect the presence of authentic Splash protein and is nonspecific.

Wheat germ agglutinin—Wheat germ agglutinin (WGA) selectively binds to N-acetylglucosamine and N-acetylneuraminic acid (sialic acid) residues. It labels neuronal elements in the CNS of insects (Jacobs and Lakes-Harlan, 1997) but to our knowledge has not been used for labeling in the CNS of crustaceans.

Amaranthus caudatus lectin—ACL preferentially binds to oligosaccharide residues containing galactosyl (β-1,3) N-acetylgalactosamine. To our knowledge, it has not been used for labeling in the CNS of insects or crustaceans.

Soybean agglutinin—Soybean agglutinin (SBA) preferentially binds to oligo-saccharide residues with terminal N-acetylglucosamine and to a lesser extend to galactose residues. It labels neuronal elements in the CNS of insects (Jacobs and Lakes-Harlan, 1997) but to our knowledge has not been used for labeling in the CNS of crustaceans.

Helix pomatia agglutinin—*Helix pomatia* agglutinin (HPA) selectively binds to α-N-acetylgalactosamine residues. To our knowledge it has not been used for labeling in the CNS of insects or crustaceans.

Confocal microscopy and image processing

To generate micrographs, fluorescently labeled sections were viewed and imaged in a confocal microscope with two-photon attachment (LSM 510; Zeiss, Jena, Germany) using the associated software package. The 488-nm line of an argon laser was used to excite and visualize AlexaFluor-488-labeled secondary antibodies or lectins as well as fluorescein-labeled lectins; the 568-nm line of a helium–neon laser was used to excite and visualize Cy3-labeled secondary antibodies; a titanium–sapphire two-photon laser tuned to 800 nm was used to excite and visualize Hoechst 33258. Stacks of 0.3–1.0-μm-thick optical sections covering the entire section thickness of 80 μm were collected. Substacks of these optical sections were collapsed to produce single two-dimensional images. The digital images were processed by filtering out high-frequency noise and by adjustment of brightness and contrast in Image Pro Express 4.5.1.3 before they were arranged into the final figures in Illustrator CS3.

RESULTS

Identification of different cell types in the olfactory deutocerebrum

We used TEM and cell-type-selective labeling with antibodies and lectins combined with labeling of all cell nuclei by the nuclear marker Hoechst 33258 to identify major cell types making up the olfactory deutocerebrum of *P. argus*. The olfactory deutocerebrum of *P. argus* is organized into two major neuropils (olfactory lobe, OL; accessory lobe, AL) composed of neuronal processes and two large clusters of neuronal somata (lateral soma cluster, LC; medial soma cluster, MC) per hemibrain. These major compartments were readily identifiable by various labeling methods, including labeling all cell nuclei with the nuclear marker Hoechst 33258 combined with labeling of synaptic areas within neuropils by anti-Syn (Fig. 3A–C). Hoechst labeling revealed the LC and MC as dense accumulations of nuclei among which the nuclei of neuronal somata are the most numerous and are characterized by an almost spherical shape and medium to intense labeling. Numerous nuclei with other shapes and more intense Hoechst labeling are interspersed with the neuronal nuclei; these belong to different cell types, perivascular cells forming the walls of arterioles and glial cells. The synaptic areas within the OL and AL neuropils were revealed by labeling with anti-Syn. Both neuropils contain only relatively few nuclei labeled by Hoechst 33258, and these are arranged in particular patterns, along arteries in the OL and AL and along the borders between the neuropil layers in the AL. In addition, both neuropils are surrounded by a dense layer of intensely Hoechst-labeled nuclei of various shapes and sizes, all of which belong to either perivascular cells or diverse types of glia.

Neurons—In the LC, somata of mature neurons were readily identifiable by TEM (Fig. 3D,E), because they are by far the most prevalent cellular structures within this compartment (Schmidt and Ache, 1994; Schmidt, 2007a). They have a regular, slightly polyhedral cell shape (FD: 12.83 ± 0.98 μm; R: 0.78 ± 0.03; n = 8) and contain an almost spherical nucleus (FD: 9.07 ± 0.38 μm; R: 0.86 ± 0.02) surrounded by a broad rim of cytoplasm, resulting in a low nuclear:cytoplasmic ratio (0.60 ± 0.25; Fig. 4). The electron-lucent and finely granulated nucleoplasm contains a large nucleolus typically in a central location and small spots of electron-dense heterochromatin that are located mostly at the periphery. The two nuclear membranes are of similar electron density, and the gap between them is relatively broad and of variable thickness. The electron-lucent cytoplasm contains many small mitochondria, numerous cisternae of rough ER that are often expanded and then appear electron lucent, numerous free polyribosomes, some large Golgi apparatuses, and a few vesicles of medium electron density likely representing lysosomes.

In our screen of antibodies and lectins, we identified WGA as a highly selective neuronal marker for the brain of *P. argus*. WGA labeled all neuropils, fiber tracts, and soma clusters but no other structures (Fig. 3F,G). Labeling intensity was considerably higher in neuropils than in fiber tracts and soma clusters. Analysis of WGA labeling in soma clusters revealed that the cell membrane of all neurons was intensely WGA^+ and that the cytoplasm of some neurons contained WGA^+ material with punctate distribution. WGA labeling of neuronal cell membranes provides a ready interpretation of the very high intensity of WGA labeling in neuropils, insofar as these are the compartments with the highest density of neuronal membranes (Sandeman and Luff, 1973).

Cell body glia—Within the LC and MC of *P. argus*, putative glial cells were first identified based on methylene blue staining of semithin sections (Schmidt, 2007a). Because of their sparse but quite regular distribution within the LC and MC, these cells were readily identifiable by TEM and by labeling with anti-pH3 and anti-Gs/olf. The somata of these cells were readily identifiable by TEM, having a nucleus and cytoplasm of markedly higher

electron density than neuronal somata (Fig. 3H,I). From the soma, several thin processes extend in different directions, resulting in an astrocyte-like cell shape. These processes form thin sheaths around individual neuronal somata, bundles of primary neurites, and the outer surface of perivascular cells forming the wall of arteries (Fig. 3J). We conclude, based on these morphological criteria, that the cells in question have a glial morphology and correspond to a class of glial cells residing in neuronal soma clusters of the insect CNS (cell body glia: Hoyle, 1986; cortex glia: Awasaki et al., 2008; Doherty et al., 2009). We use the term *cell body glia* for cells of this type. At least one but usually several closely attached layers of processes of cell body glia separate neuronal somata from each other and from perivascular cells. The processes of cell body glia are distinct from the cells they surround by having higher electron density and by containing flat cisternae of rough ER that are very electron dense. Cell body glia are differentiated into two distinct types (Figs. 3H,I, 4). Type 1 cell body glia have a large, spherical or irregularly shaped soma (FD: 10.82 ± 2.51 μm; R: 0.61 ± 0.19; n = 11) and contain an almost spherical nucleus (FD: 7.76 ± 1.76 μm; R: 0.76 ± 0.11) surrounded by a broad rim of cytoplasm, resulting in a low nuclear:cytoplasmic ratio (0.65 ± 0.27). Type 2 cell body glia have a small soma of irregular shape (FD: 5.64 ± 1.32 μm; R: 0.42 ± 0.13) that contains an irregularly shaped nucleus (FD: 4.60 ± 1.30 μm; R: 0.59 ± 0.09) surrounded by a very thin rim of cytoplasm, resulting in a high nuclear:cytoplasmic ratio (1.47 ± 1.01). The nucleus of type 1 cell body glia has finely granulated nucleoplasm, a large central nucleus, and very little peripheral heterochromatin. The cytoplasm of type 1 cell body glia contains numerous large mitochondria with low electron density, numerous free polyribosomes, some Golgi apparatuses, and extensive cisternae of rough ER, which are very robust and of very high electron density. The nucleus of type 2 cell body glia contains large areas of very electron-dense heterochromatin and one central or two peripheral nucleoli. The cytoplasm of type 2 cell body glia contains some free polyribosomes and extensive cisternae of rough ER, which are very robust and of very high electron density.

In our screen of antibodies and lectins, we identified anti-pH3 as a highly selective and anti-Gs/olf as a moderately selective marker for cell body glia (Figs. 3K–M, 6A–F, 10L–N). Both antibodies labeled cell body glia in the MC and LC and cells with similar morphology in other neuronal soma clusters, in nerve roots, and in the vicinity of neuropils. The labeling was cytoplasmic and allowed visualization of the beginning of the processes extending from the soma. From these findings, we conclude that cell body glia are present in all neuronal soma clusters but are not restricted to them. In addition to labeling cell body glia, anti-pH3 also labeled M-phase nuclei in the neurogenic complexes (see below; Fig. 5A,B,D). As detailed in Materials and Methods, we conclude that the labeling of cell body glia obtained with anti-pH3 was likely nonspecific. In addition to labeling cell body glia, anti-Gs/ olf labeled the cell membranes of all cells in the neurogenic complexes except for aNBs and the cells located in the duct. This allowed a direct visualization of the spatial arrangement of the different compartments (clump of cells, duct, proliferation zone) of the neurogenic complexes (Fig. 6A–F).

Neuropil glia—Immunocytochemical labeling with anti-GS, which is used a selective marker for astrocytes in vertebrates (Norenberg, 1979; Hertz et al., 1999), identified a particular class of glial cells in the olfactory deutocerebrum of *P. argus* with somata at the edge of neuropils and processes extending into the neuropils (Linser et al., 1997).

Previously, Orona et al. (1990) described cells with similar morphology as putative glial cells based on labeling with antihistamine, but, because antihistamine also labels a class of local interneurons (whose somata are located in the MC) in the olfactory deutocerebrum of *P. argus* (Wachowiak and Ache, 1997), it does not represent a glia-specific marker. In our screen of antibodies and lectins, we identified anti-GS (No. 610518; BD Biosciences) as a

highly selective marker for glial cells with the morphological features described by Linser et al. (1997). Most GS^+ glial cells had a soma located at the edge of a neuropil and were of unipolar morphology, extending one thick process toward the neuropil; only a small percentage of GS^+ somata at the edge of a neuropil had two or more processes (Fig. 3N,O). The main processes penetrated the neuropil, often running along arterioles before they branched extensively, giving rise to very fine terminals that evenly filled the entire neuropil volume. All neuropils of the brains were surrounded by GS^+ glial cells. Among these neuropils, the OL stood out, because in the GS^+ glial cells in its surround the intensity of immunostaining was distinctly lower than in the other neuropils. Some GS^+ glial cells had their soma farther away from neuropil areas. Typically, these cells were multipolar, extending three or more main processes in different directions (Fig. 3P). Most of these processes projected into neuropils but some could not be traced that far. The nucleus of all GS^+ glial cells had a very regular, spherical to slightly elliptical shape and was labeled with medium intensity by Hoechst 33258 (Fig. 3O,P). Hoechst labeling of all nuclei revealed that only a minor percentage (<10%) of the cell somata present at the edge of neuropils is GS^+. The nuclei of GS^- cells were of diverse shapes and sizes and often showed a higher intensity of Hoechst labeling. Typically, the nuclei of GS^- cells were smaller and less spherical than the nuclei of GS^+ glial cells.

Analysis of the tissue composition at the edge of the OL with TEM revealed the presence of many cells that are not perivascular cells surrounding the lumen of arterioles and hence must be glia (Fig. 3Q). Among these putative glial cells, at least four different types could be distinguished based on pronounced differences in cell shape, nuclear ultrastructure, and cytoplasmic composition. One type corresponds to GS^+ glial cells in morphology and frequency of occurrence (<10%). These cells have a very regularly shaped round or slightly elliptical nucleus, a broad rim of cytoplasm, and one major process extending from the soma toward the neuropil (Fig. 3R). The nucleus of these cells contains small, mostly peripheral accumulations of heterochromatin and a small, eccentric nucleolus; both nuclear membranes are very closely attached to each other, and the gap between them is very constant in width. The cytoplasm of these cells is of medium electron density and contains numerous small mitochondria of medium electron density, many tight cisternae of rough ER, and some small Golgi apparatuses. We tentatively identify the cells with these ultrastructural features as the GS^+ glial cells and propose the term *neuropil glia 1* for them to distinguish them from other types of putative glial cells residing at the rim of neuropils.

Arterioles and perivascular cells—The brain of decapod crustaceans is supplied with hemolymph via the cerebral (or median) artery that branches into an extensive tree-like system of major and then finer arterioles. The arterioles pervade all neuropils and soma clusters, albeit with highly variable density (Fig. 10A,B; Sandeman, 1967; Abbott, 1971). In the LC and the MC of *P. argus*, arterioles were readily identifiable by TEM as mostly empty extracellular spaces completely surrounded by flat processes of cells with unique ultrastructural properties (Fig. 3S–U). Following the terminology of Abbott (1971), we use the term *perivascular cells* for these cells, because it is not established whether they are of mesodermal origin and represent true endothelial cells or are of ectodermal origin. Perivascular cells are characterized by having a flattened nucleus of irregular shape (FD: 4.89 ± 0.81 μm; R: 0.60 ± 0.15; n = 14; Fig. 4B,E) and a finely granulated cytoplasm of low or medium electron density. The nucleus is often bent, following the outline of the arteriole lumen, and usually has one or several extensive invaginations. The nucleoplasm is finely granulated and contains peripheral accumulations of very electron-dense heterochromatin and in some cells a central nucleolus. The cytoplasm contains numerous small mitochondria of medium electron density and some cisternae of rough ER. The perivascular lining of the arteriole lumen consists of at least two but usually more highly overlapping processes of perivascular cells stacked upon each other. The luminal surface of the innermost

perivascular cell process is covered by a continuous basal lamina that is 30–60 nm thick but contains numerous conspicuous bulges with a thickness of up to 350 nm (Fig. 3J,T,U). The basal lamina consists of unstructured, flocculent material of medium electron thickness and sometimes carries very electron-dense spherical particles on its luminal surface. The arteriole lumen appears mostly as electron-lucent empty space, most likely because the hemolymph it normally contains was flushed out during perfusion fixation. Occasionally, the arteriole lumen contains aggregates of electron-dense particles and hemocytes that, by having large electron-dense granules (FD: 1.00 ± 0.15 μm; n = 9) in the cytoplasm, are characterized as typical crustacean granulocytes (Hose et al., 1990). Most arteriole profiles in the MC and LC are simple (Fig. 3U), but several are complex, appearing as a vessel within a vessel (Fig. 3S,T). These profiles correspond to type 2 and type 1 profiles described by Abbott (1971b), respectively. Complex arterioles have an inner lumen surrounded by an inner ring of perivascular cells and an outer lumen that surrounds the inner ring of perivascular cells and is itself surrounded by an outer ring of perivascular cells. All luminal surfaces of the inner and outer perivascular cells are covered by a continuous basal lamina. The perivascular cells that form the inner and outer ring do not consistently differ in cellular appearance or the ultra-structure of their basal lamina, suggesting that they do not represent different cell types.

In our screen of antibodies and lectins, we identified ACL as a moderately selective marker for perivascular cells in the brain of *P. argus*. ACL intensely labeled arterioles, small dots within the cytoplasm of neuronal somata, and fine (neuronal or glial) processes within neuropils. In the LC and MC, the ACL^+ arterioles stood out because of a continuous and distinctly higher intensity of labeling than present in neuronal somata (Figs. 3V, 6B,D, 10F–H). The ACL^+ dots in the cytoplasm of neuronal somata most likely represent mitochondria, insofar as these are the only organelles that, according to TEM, have a corresponding size, number, and distribution. Interestingly, ACL did not label cells in the proliferation zones (Fig. 6B), making it a potentially useful marker for distinguishing mature from immature neurons located in the periphery of the proliferation zone (see below).

Triple labeling of cells in the neurogenic complexes with anti-BrdU, anti-pH3, and Hoechst 33258

With the optimized DNase digestion protocol, we routinely achieved triple labeling in the neurogenic complexes in the LC and MC of *P. argus* brains with anti-BrdU, anti-pH3, and Hoechst 33258 or double labeling with anti-BrdU and Hoechst 33258 (Fig. 5A–E). This allowed visualization of all cell nuclei ($Hoechst^+$) and determination of which of them were in S-phase of the cell cycle at the time when BrdU was available for incorporation into newly synthesized DNA ($BrdU^+$) and (in brains triple labeled with anti-pH3) which were in M-phase of the cell cycle at the time of fixation ($pH3^+$). Hoechst labeling clearly identified the proliferation zone, the clump of cells, the aNB it contains, and the duct connecting the clump of cells with the proliferation zone. The proliferation zone localized at the interior margin of both soma clusters was characterized by containing irregularly shaped small nuclei at a distinctly higher nuclear density than present in the surrounding area containing less densely packed and almost spherical nuclei of mature neuronal somata. The clump of cells located at a characteristic position with respect to the proliferation zone (LC: 70–100 μm posteriorventrally from the proliferation zone; MC: 50–70 μm anteriormedially from the proliferation zone) was characterized by being composed of small and irregularly shaped nuclei that were very intensely labeled by Hoechst and formed a compact accumulation with distinct spherical (LC) or elliptical (MC) shape (Fig. 5B,C,E). At the pole facing the associated proliferation zone, the clump of cells contained the markedly larger, more regularly shaped (round or slightly elliptical), and less intensely Hoechst-labeled nucleus of the aNB (Fig. 5J, inset, L, inset). In one LC, the Hoechst-labeled and $BrdU^+$ aNB was

captured in telophase of mitosis (Fig. 5C, inset). The duct connecting the clump of cells with the proliferation zone was characterized by forming a tunnel devoid of the spherical nuclei of mature neuronal somata surrounding it (Fig. 5B,C).

In contrast to two previous studies based on in vivo BrdU labeling, here single BrdU injections were administered in the morning and followed by relatively short survival times of 2–10 hours (2 hours: n = 3; 4 hours: n = 1; 6 hours: n = 5; 9–10 hours: n = 9 animals) to elucidate which cell cycle parameters control BrdU incorporation by aNBs. In one of the previous studies, multiple BrdU injections over a 48-hour period resulted in the consistent labeling of aNBs by BrdU (Schmidt, 2007a); in the other study, single BrdU injections administered in the evening and followed by 14 hours survival time did not result in labeling of aNBs by BrdU (Schmidt, 2001). In the present experiment, a significant percentage of aNBs was $BrdU^+$ including in brains fixed after a survival time of only 2 hours (Fig. 5A–E). Overall, 82% of the aNBs in the LC (27 of 33 LCs that could be analyzed; three LCs were lost or damaged during tissue processing) and 50% of the aNBs in the MC (17 of 34 MCs that could be analyzed; two MCs were lost or damaged during tissue processing) were $BrdU^+$. BrdU labeling intensity varied widely between aNBs independent of survival time. In line with previous reports (Schmidt and Harzsch, 1999; Schmidt, 2001), the proliferation zones of all MCs and LCs that could be analyzed contained a densely packed group of small, robustly $BrdU^+$ nuclei of neuronal progenitor cells (Fig. 5A,B,D). Within each group, BrdU labeling intensity was variable, and in addition we observed an overall lower intensity of BrdU labeling after the shortest survival time of 2 hours. In a few cases, one or two large, slightly elongated nuclei located in the duct were $BrdU^+$, as was also found after multiple BrdU injections over a 48-hour period (Schmidt, 2007a). We did not observe any $BrdU^+$ nuclei in the clumps of cells other than those of aNBs.

In all brains triple labeled with anti-pH3 (n = 12), some nuclei in the neurogenic complexes were intensely $pH3^+$, and these $pH3^+$ nuclei were located in two characteristic positions as was reported previously (Schmidt, 2007a). In all analyzed LCs and in most MCs, at least one and up to three (MC) or seven (LC) $pH3^+$ nuclei were located in the innermost aspect of the proliferation zone, farthest away from the associated clump of cells (Fig. 5A,B,D). In one LC, the aNB was $pH3^+$, but in no instance was a $pH3^+$ nucleus present in the duct or in any other region of the soma clusters. The $pH3^+$ nuclei were condensed, were of irregular shape, and in several cases were arranged as opposing pairs as is typical for nuclei in various phases of mitosis (metaphase, anaphase, telophase). In brains with survival times from 2–6 hours, none of the $pH3^+$ nuclei was also $BrdU^+$; in brains with survival times of 9–10 hours, some of the $pH3^+$ nuclei in the proliferation zones of both soma clusters were also weakly $BrdU^+$. Anti-pH3 reliably labeled not only M-phase nuclei in the neurogenic complexes but in addition a sheath of fibrous material surrounding the clump of cells and the duct arising from it (Fig. 5A–D). As detailed in Materials and Methods, we conclude that the labeling of the fibrous material by anti-pH3 was likely nonspecific (see also Schmidt, 2007a).

Ultrastructure of neurogenic complex in the lateral soma cluster

To elucidate the ultrastructural organization of the neurogenic complex in the LC, series of ultrathin sections from three brains of adult *P. argus* were analyzed. In each case, the main compartments of the neurogenic complex—the clump of cells, the proliferation zone, and the duct connecting both structures—could readily be identified based on their specific locations and peculiar cytoarchitecture.

Clump of cells: clump-forming cells—The clump of cells consists of an almost continuous cortex of somata of a peculiar cell type for which we use the term *clump-forming cells* (CFCs; Figs. 6I,J, 7G–N). The somata of CFCs are small and of irregular shape (FD:

4.45 ± 0.78 μm; R: 0.63 ± 0.12; N = 40), and they contain a relatively large nucleus of highly irregular shape (FD: 3.91 ± 0.75 μm; R: 0.57 ± 0.12) surrounded by a very thin layer of cytoplasm resulting in a high nuclear:cytoplasmic ratio (2.23 ± 0.67; Fig. 4). The cytoplasm is distinctly more electron dense and more finely granulated than the cytoplasm of neuronal somata and contains numerous small mitochondria as well as extensive cisternae of rough ER that are more delicate than those of cell body glia (Figs. 7I, 8G,H). The nucleus of many CFCs is characterized by one or more deep invaginations (Fig. 7J,M,N). The nucleoplasm is of medium electron density and is composed of a peripheral layer of more electron-dense heterochromatin that sometimes contains one or two nucleoli of very high electron density. The only opening in the cortex of CFC somata is formed by the nucleus-containing, main domain of the aNB located at the apex of the clump of cells facing toward the adjacent proliferation zone (Figs. 6H, 7A). Each CFC soma has two sheath-like and very irregularly shaped processes, a short one reaching into the center of the clump of cells and a long one projecting outward. The long processes wrapping around each other in many convoluted layers together fill the interior of the duct connecting the clump of cells with the adjacent proliferation zone (Figs. 6G, 8D), leaving only little extracellular space. The inward facing, short processes of the CFCs also wrap around each other in many convoluted layers and fill the entire center of the clump of cells, except for a roughly spherical space located in the apex-opposing aspect of the clump of cells (Figs. 6I, 7C). This space is filled by the bulbous foot of the aNB, and collectively the inward facing processes of the CFCs completely cover it (Fig. 7C–E). Processes of all CFCs appear to reach the bulbous foot of the aNB and participate in the formation of this continuous cover, but, because of the extremely convoluted contours of the CFC processes, this could not be delineated with certainty. At the interface between CFC processes and the bulbous aNB foot, the cell membranes of both cell types are smooth and regular and do not show any obvious specializations. Rarely, small membrane specializations resembling desmosomes (widened intercellular cleft filled by electron-dense material) are present between adjacent CFCs in the vicinity of the bulbous foot of the aNB (Fig. 7E,F).

Clump of cells: aNB—The nucleus-containing domain of the aNB is located at the apex of the clump of cells facing toward the adjacent proliferation zone, and it is distinctly larger than the CFC somata (Figs. 6H, 7A). It is completely surrounded by the somata and outward-facing processes of CFCs. The cytoplasm of the aNB differs distinctly from the cytoplasm of the surrounding CFCs in being less electron-dense and in containing numerous electron-dense granules that have the size and appearance of glycogen granules (Fig. 7A,B). In addition, the aNB cytoplasm contains some small ER cisternae and many large, electron-lucent mitochondria. The nucleus of the aNB has a relatively smooth, slightly elliptical shape and is characterized by a thin seam of peripheral heterochromatin and one very large peripherally located nucleolus of high electron density (Figs. 6H, 7A). Aided by the unique appearance of the aNB cytoplasm, we traced a thin process extending from the peripheral nucleus-containing domain of the aNB into the center of the clump of cells through series of ultrathin sections. In the center of the clump of cells, this process expands dramatically and forms a smooth, bulb-shaped end-foot (Figs. 6I, 7C,D). The cytoplasm of this bulbous foot is indistinguishable from that of the peripheral, nucleus-containing domain of the aNB. Thus, the aNB has a highly unusual hourglass-like shape, with two almost equally large domains that are connected by a thin cytoplasmic process.

Duct—The duct that arises at the apex of the clump of cells and is filled by the bundled and highly convoluted processes of CFCs extends into and penetrates the adjacent proliferation zone (Figs. 6G, 8A,D). Within the proliferation zone, the duct gradually widens, and the processes of CFCs separate into smaller strands of tissue that become thinner until they cannot be traced farther. The duct contains several large cells with elliptical, oblong shape

(elongated in the long axis of the duct) resembling the aNB in cytoplasmic appearance. These cells are completely surrounded by CFC processes. They have a smooth nucleus that lacks a conspicuous nucleolus and is characterized by extensive peripheral and central heterochromatin. Close to the clump of cells, these oblong cells are clearly separated from each other by intervening stretches of duct that are devoid of them. Toward the proliferation zone, the frequency of cells enclosed by the duct increases, and these cells overlap with one another. With increasing distance from the clump of cells, the cells enclosed in the duct also gradually change their cytoplasmic and nuclear appearance and become indistinguishable from the surrounding cells of the proliferation zone.

Proliferation zone—The proliferation zone is densely populated by small cells, among which three types can be distinguished (Fig. 9). Type A cells are least numerous, very small, and of somewhat irregular shape (FD: 5.73 ± 0.90 μm; R: 0.68 ± 0.10; N = 11). They contain a relatively large nucleus of slightly irregular shape (FD: 5.13 ± 0.87 μm; R: 0.73 ± 0.10) surrounded by a very thin rim of cytoplasm resulting in a very high nuclear:cytoplasmic ratio (2.57 ± 0.59; Figs. 4, 9A,C–E). The cytoplasm is of medium electron density and contains numerous fine granules and some mitochondria but no other organelles. The nucleoplasm contains a small, peripheral nucleolus and large aggregates of heterochromatin with medium electron density, and both nuclear membranes are very tightly attached to each other. Occasionally, cells with the cytoplasmic and nuclear features of type A cells were captured in anaphase or telophase of mitosis (Fig. 9E). Type B cells are the most numerous cells in the center of the proliferation zone. They are slightly larger and have a more irregular shape than type A cells (FD: 6.02 ± 1.17 μm; R: 0.63 ± 0.12; N = 17), and they have a broader rim of cytoplasm surrounding the nucleus, resulting in a lower nuclear:cytoplasmic ratio (1.73 ± 0.65; Figs. 4, 9A,B,F,G). The cytoplasm contains several mitochondria that are electron lucent and some small ER cisternae. The most distinctive feature of type B cells is their mostly elliptical nucleus (FD: 5.13 ± 1.17 μm; R: 0.74 ± 0.10; Fig. 4) that is filled by homogeneous, finely granulated nucleoplasm containing a small peripheral nucleolus. The inner nuclear membrane is distinctly thicker and more electron dense than the outer one, and both nuclear membranes are separated by a small and very regular gap. Type C cells are larger and of more regular shape than type B cells (FD: 9.46 ± 1.32 μm; R: 0.77 ± 0.05; n = 10) and are located mostly in the periphery of the proliferation zone (Figs. 4, 9A,H). In nuclear and cytoplasmic appearance, type C cells resemble somata of mature neurons, but they are smaller and have a thinner rim of cytoplasm, resulting in a higher nuclear:cytoplasmic ratio (0.90 ± 0.26). Their nucleus is of regular, slightly elliptical shape and contains coarsely granulated, electron-lucent nucleoplasm with mostly peripheral heterochromatin of very high electron density and at least one central or peripheral nucleolus. The gap between the two nuclear membranes is distinctly broader and less regular than in type B cells. The cytoplasm of type C cells is more electron lucent than that of type A or B cells, and it contains fine granules; some electron-lucent ER cisternae; several large, electron-lucent mitochondria; and some electron-dense vesicles. A distinctive morphological feature of the central area of the proliferation zone is that type A and type B cells are in direct contact with each other (Fig. 9B). Their cell membranes are not separated by interspersed processes of cell body glia. A similar lack of glial ensheathment was reported for neuronal progenitor cells located centrally in the cluster of mature Kenyon cell somata in the mushroom bodies of adult crickets (Mashaly et al., 2008). Type C cells in the periphery of the proliferation zone are at least partially and in many cases completely surrounded by a thin layer of electron-dense tissue consisting of processes of cell body glia (Fig. 9H).

Glial envelope and associated arteriole—The clump of cells and the interior of the duct arising from it—until it reaches the proliferation zone—are completely enveloped by a layer of electron-dense tissue separating them from other tissue components. This layer

consists of processes of cell body glia originating from cell body glia somata of types 1 and 2 located in the immediate vicinity of the clump of cells and the duct (Figs. 6J, 8A,B). The entire glial envelope is formed by many highly overlapping processes of cell body glia, but it varies considerably in overall thickness (60 nm to 2 μm) as well as the thickness and number of layers of glial cells contributing to it (Fig. 8D–H). A minimum of one and maximally 10 cell body glia processes stacked on top of each other constitute the envelope. A single layer can be exceedingly thin (<20 nm), with no discernable cytoplasmic space between the cell membranes (Fig. 8F,H), or be much thicker (up to 300 nm) and then contain the typical cytoplasmic components of cell body glia, in particular the robust and very electron-dense cisternae of rough ER (Fig. 8D,G). When the duct reaches the proliferation zone, the glial envelope separates into several very irregularly shaped sheaths of tissue. These glial sheaths are mostly interspersed between cells in the inner and the peripheral region of the proliferation zone, but they do not constitute a continuous and well-demarcated boundary between these regions (Figs. 8A, 9A,C–E,H).

The clump of cells is attached to an arteriole of fairly large width (maximum diameter ~15 μm; Figs. 6H,I, 8C). This arteriole runs along the duct until it reaches the proliferation zone and then separates from it and becomes gradually thinner (Fig. 6G). The arteriole is insulated from the somata and processes of CFCs by the glial envelope formed by the processes of cell body glia (Fig. 8C–F). We did not find a consistent difference in the thickness or in the number of glial cell layers of the glial envelope between regions where neuronal somata are attached to the clump of cells (Fig. 8G,H) and regions where the arteriole is attached to it (Fig. 8C–F).

Perfusion of fluorescent dextrans into cerebral artery

To test whether hemolymph has access to the interior of the clump of cells, we perfused fluorescent dextrans of different molecular weights (3,000 or 10,000) into the brain of *P. argus* via the cerebral artery and immediately afterward fixed the brain by immersion in fixative. In the brain of treated animals (N = 4, 2 for each dextran), the branched system of arterioles was intensely labeled in neuropils and in some soma clusters, including those of the olfactory deutocerebrum (Fig. 10A,B). The olfactory deutocerebrum of each hemibrain receives a major arteriole branch penetrating the area between OL and AL from dorsally. This large arteriole enters the fibrous core of the OL through the anterior foramen, which also accommodates the passage of primary neurites of local interneurons whose somata are located in the MC. In the core of the OL, the large arteriole branches out into a tree-like system of ever smaller arterioles densely permeating the OL cortex and into several medium-sized arterioles that supply the AL, LC, and MC (Fig. 10A). The OL cortex consists of wedge-shaped olfactory glomeruli (Schmidt and Ache, 1997; Schachtner et al., 2005), but the dense arteriole branches appear not to respect glomerular boundaries. In the AL, medium-sized arterioles run in the two interfaces between the three neuropil layers (lateral-central layer interface, central-medial layer interface), and from there branch out into finer vessels permeating the lateral and medial layer. The MC and LC are penetrated by medium-sized arterioles from their inner surfaces facing toward the OL neuropil. The arterioles branch out toward the periphery of the soma clusters, but these branches do not become continuously thinner and are often interconnected, resulting in an overall net-like topography (Fig. 10B). This arteriole net is denser and more elaborate in the LC than in the MC. In both soma clusters, the proliferation zone is penetrated by only one arteriole and thus is distinctly less vascularized than the surrounding area (Fig. 10B). The clump of cells is invariably attached to an arteriole. This arteriole does not penetrate the clump of cells, nor does it terminate at it. In no case did we observe dextran labeling within the clump of cells, when either the 3,000- or 10,000-MW dextran was perfused into the cerebral artery (Fig.

10C–E). The neuropils and soma clusters are surrounded by very large, but diffuse hemolymph sinuses, into which the fine end-branches of arterioles terminate (Fig. 10B).

Identification of cell types in the neurogenic complexes by selective labeling

To gain information about the cellular identity of the cells constituting the different compartments of the neurogenic complexes independent of their ultrastructural features, we analyzed whether and how they were labeled by those markers (antibodies, lectins) that we identified as selective markers of certain cell types in the olfactory deutocerebrum of *P. argus* (see above). Of greatest interest in this analysis were the CFCs, because their cellular identity cannot be determined simply from location and overall cell shape.

Neuronal markers—WGA, which we identified as a highly selective neuronal marker (Fig. 3F,G), did not label the CFCs (cortex of clump of cells and duct) or the cells in the proliferation zone (Fig. 10J,K). From the proliferation zone outward, WGA labeling of soma membranes became progressively more intense. The labeling of dots (likely representing mitochondria) in the cytoplasm of somata by ACL showed a similar progression in intensity. This suggests that, in somata surrounding the proliferation zone, WGA and ACL binding is a function of neuronal maturation.

Glial markers—We identified anti-GS as a highly selective and likely specific marker for neuropil glia 1 (Fig. 3N–P), confirming previous reports from *P. argus* (based on labeling with a different antibody against GS) and from other decapod crustaceans (based on labeling with the same anti-GS as was used here; Sullivan and Beltz, 2005b; Sullivan et al., 2007a; Harzsch and Hansson, 2008). In our experiments, anti-GS selectively labeled neuropil glia 1 cells at the rim of neuropils, including the OL and AL, but it did not label any structures within the soma clusters of the brain, including the neurogenic complexes in the MC and LC (Fig. 10I,K). Thus in *P. argus*, all cell types present in the neurogenic complexes, including the CFCs, are GS^{-}.

We identified anti-pH3 as a selective marker of cell body glia (in addition to being a specific marker of nuclei in M-phase of the cell cycle; Fig. 3K–M). Anti-pH3 intensely labeled the somata and main processes of cell body glia in the MC and LC and in addition a sheath of fibrous material surrounding the clump of cells and the duct, which was described previously based on labeling with the same anti-pH3 (Schmidt, 2007a). We observed several $pH3^{+}$ somata of cell body glia in the vicinity of the clump of cells and the duct with processes that extended into the $pH3^{+}$ fibrous sheath surrounding them (Fig. 10L–N). This arrangement is congruent with the results of our electron microscopic analysis showing that processes of cell body glia form a continuous, multilayered sheath around the clump of cells and the duct. Thus within the neurogenic complexes, anti-pH3 selectively labeled the glial sheath but no other cell types, including CFCs.

Somata and processes of cell body glia in the MC and LC were also labeled by anti-Gs/olf, but this labeling was not selective; anti-Gs/olf also labeled the cell membranes of CFCs and of cells in the proliferation zone (Fig. 6A,D–F). This distribution of labeling indicates that the three most numerous cell types forming the neurogenic complexes share an epitope to which anti-Gs/olf binds. However, our Western blot results indicate that this epitope may not represent an authentic Gαs subunit, insofar as, in *P. argus* brain extracts, protein bands of distinctly higher than predicted molecular weight were intensely labeled by anti-Gs/olf (Fig. 2A). Labeling with anti-Gs/olf highlighted the entire neurogenic complex, but it did not provide additional information about the cellular identity of the CFCs.

Perivascular cell marker—We identified ACL as a moderately selective marker for perivascular cells. In the MC and LC, labeling with ACL differentiated the net-like system of arterioles that was also labeled after perfusion of fluorescent dextrans into the cerebral artery from neuronal somata (Figs. 3V, 10F). This differentiation was due to an intense and continuous labeling of the cytoplasm of perivascular cells by ACL that was in clear contrast to the punctate ACL labeling of neuronal somata (Figs. 6B,D, 10G,H). The neurogenic complexes of MC and LC were completely devoid of ACL labeling (Figs. 6B,D, 10F–H). Thus, none of the cell types present in the neurogenic complexes of *P. argus*, including the CFCs, shares "ACL-specific" carbohydrate residues with perivascular cells (or mature neurons). ACL labeling of the arterioles within the MC and LC confirmed that in both soma clusters the clump of cells is attached to an arteriole and that there is no contiguity between the two structures (Fig. 10G,H).

Selective labeling of the interface between the bulbous foot of the aNB and CFCs

Aside from anti-BrdU and anti-pH3, none of the >150 probes that we screened for labeling components of the neurogenic complexes labeled the main, nucleus-containing domain of the aNB located at the apex of the clump of cells. In contrast, four of these probes (anti-Splash, SBA, WGA, HPA) intensely labeled the region in the center of the clump of cells that according to our electron microscopic analysis is occupied by the bulbous foot of the aNB (Fig. 5F–L). For anti-Splash and SBA, labeling of this region in the center of the clump of cells was highly selective; neither probe labeled any other structures in the brain (Fig. 5F,G,J,K). Within the neurogenic complexes, WGA exclusively labeled the region in the center of the clump of cells (Fig. 10J,K), but in addition WGA also labeled all neurons (see above). Within the neurogenic complexes, HPA labeled exclusively the region in the center of the clump of cells (Fig. 5H,L). In addition, HPA intensely labeled neuropil regions and weakly labeled neuronal somata in a dot-like pattern (similar to ACL labeling). Double labeling with anti-Splash and SBA or with anti-Splash and HPA revealed that the regions labeled by each of the two probes were concentric, with very little overlap (Fig. 5J–L). In each case, a $Splash^+$ ring surrounded a center that was SBA^+ or HPA^+. The labeled center was almost spherical, and its rim was labeled more intensely than its core. We conclude, based on the electron microscopic analysis of the interior of the clump of cells, that labeling likely is located at the interface between the bulbous foot of the aNB and the attached processes of CFCs. The concentric distribution of labeling indicates that $Splash^+$ material is located in the terminals of the inner processes of CFCs, whereas the material that is SBA^+, HPA^+, and WGA^+ is located in the bulbous foot of the aNB and concentrated at its cell membrane.

DISCUSSION

The detailed analysis of the cytoarchitecture of the neurogenic complexes in olfactory deutocerebrum of adult spiny lobsters, *P. argus*, based on TEM and labeling with cell-type-selective markers leads to the conclusion that the clump of cells associated with each proliferation zone fulfills morphological criteria of a stem cell niche. The clump of cells is composed of bipolar cells with unique ultrastructure, clump-forming cells (CFCs). Collectively the CFCs form a continuous envelope around the hourglass-shaped aNB, separating it from other tissue components, and thereby the CFCs solely constitute the aNB microenvironment. The clump of cells is intimately associated with glial and vascular elements and thus has structural parallels with NSC niches in the brain of adult mammals. Through BrdU pulse-chase experiments with short survival times, we provide evidence that the aNBs cycle rapidly during daytime. This proliferation kinetic differs dramatically from that of NSCs maintaining adult neurogenesis in the mammalian brain, which are largely quiescent (Morsehead et al., 1994; Doetsch et al., 1999a). We propose, based on these

findings, a new model of the cell lineage and the cell movements through which the single aNB continuously repopulates the GMC-type neuronal progenitor cells in the attached proliferation zone.

NSC identity of aNBs

To allow the lifelong maintenance of adult neurogenesis in the olfactory deutocerebrum of decapod crustaceans, self-renewing NSCs must be present to replenish the pool of GMC-type neuronal progenitor in the proliferation zones, all of which ultimately undergo one terminal symmetrical cell division (Schmidt, 2001). Previously, BrdU labeling revealed that in adult spiny lobsters (*P. argus*) and crayfish (*P. clarkii*) each proliferation zone is associated with a single proliferating cell that has a distinct and invariant location, is connected to a unique clump of cells, and has a significantly larger nucleus than neuronal pregenitor cells or neurons (Schmidt, 2007a; Song et al., 2009). Since large size is the identifying feature of NBs in embryonic and larval neurogenesis of crustaceans and insects (Hartenstein et al., 1987; Harzsch, 2001; Egger et al., 2008; Boyan et al., 2010), we proposed that the single large proliferating cells are aNBs and act as NSCs (Schmidt, 2007a; Song et al., 2009). This interpretation, however, is not generally accepted, and it has been proposed alternatively that the CFCs act as NSCs (Sullivan et al., 2007a) or that in the clump of cells hemocytes transdifferentiate into neuronal progenitor cells (Zhang et al., 2009).

A defining feature of stem cells, including NSCs, is that they undergo asymmetric cell divisions in which one daughter cell persists as a self-renewed stem cell while the other daughter cell gives rise to differentiated progeny (Doe, 2008; Egger et al., 2008; Zhong and Chia, 2008; He et al., 2009). In revealing that the aNBs have a unique hourglass-like shape, the present ultrastructural analysis supports the interpretation that they act as NSCs, since this unusual morphology indicates that the aNB cell divisions are intrinsically asymmetric, giving rise to two daughter cells with distinct morphology, location, and fate. Each aNB consists of an outer domain at the apical (proliferation zone-facing) pole of the clump of cells that contains the large nucleus and an inner domain forming a bulbous foot within the clump of cells (Fig. 11A). Since the mitotic plane of the aNB nucleus is perpendicular to the long axis of the hourglass (Schmidt, 2007a; this study), the aNB cell division likely generates an outer daughter cell located in the beginning of the duct and an inner daughter cell that retains the hourglass-like shape and remains anchored in the clump of cells with its bulbous foot. In this scenario, the inner daughter cell represents the self-renewed aNB, whereas the outer daughter cell migrates through the duct to the proliferation zone and replenishes the pool of neuronal progenitor cells (Fig. 11B). Migration of the outer daughter cells to the proliferation zone is supported by direct and indirect evidence from crayfish (Sullivan et al., 2007a; Zhang et al., 2009).

With *P. argus*, we did not find evidence supporting the alternative suggestions that the CFCs act as NSCs or that neuronal progenitor cells are generated by transdifferentiating hemocytes (Sullivan et al., 2007a; Zhang et al., 2009). Neither in this study nor in previous studies were any proliferating ($BrdU^+$) CFCs identified in adult or subadult *P. argus* (Schmidt and Harzsch, 1999; Schmidt, 2001, 2007a). Thus it is highly unlikely that CFCs maintain continuous adult neurogenesis in *P. argus*, although it is possible that CFCs occasionally regenerate an aNB should its life span be limited. The possibility in *P. argus* of hemocytes transdifferentiating into neuronal progenitor cells within the clump of cells seems highly unlikely, because hemocytes present within brain arterioles have the distinct ultrastructural features of granulocytes (Hose et al., 1990) and the clump of cells does not contain cells with similar features.

Cell cycle dynamics of aNBs and neural progenitor cells

A characteristic feature of most (but not all) types of adult stem cells, including NSCs in mammalian brains, is to be largely quiescent and to divide only rarely (Morsehead et al., 1994; Doetsch et al., 1999a; Fuchs, 2009). This rare cycling is interpreted as a mechanism to minimize accumulation of DNA copy errors through consecutive rounds of semiconservative DNA replication and is evident in the retention of BrdU-labeled DNA for extended periods. To generate a sufficient number of somatic cells, quiescent stem cells coexist with active ones and/or give rise to transit amplifying intermediate progenitor cells that proliferate rapidly (Doetsch et al., 1999a; Li and Clevers, 2010). Previous experiments indicated that aNBs of *P. argus* might be somewhat quiescent because they were consistently labeled by BrdU after extended exposure to BrdU (Schmidt, 2007a) but were generally not labeled after single BrdU injections (Schmidt, 2001). However, since the single BrdU injections were administered in the evening, an alternative explanation for the conflicting results is that aNBs preferentially divide during daytime. To distinguish between the two alternatives, we used single BrdU injections administered in the morning followed by a short survival time of 2–10 hours in the present experiments. Our finding that overall 82% of aNBs in the LC and 50% of aNBs in the MC were labeled by BrdU demonstrates that most aNBs are in S-phase during daytime and that they are not quiescent. The previous failure to label aNBs by BrdU injections in the evening indicates that their S-phase ends earlier and that their entire cell cycle lasts less than 24 hours. Thus, aNBs appear to cycle quite rapidly, which is in line with the low incidence of capturing them in mitosis (Schmidt, 2007a; this study). Also in crayfish aNBs were consistently labeled by single BrdU injections followed by short survival times (Song et al., 2009), indicating that rapid cycling is a common feature of decapod crustacean aNBs. The finding that aNBs are regularly in S-phase during daytime but not at night implies that aNB cell divisions are under circadian control. Circadian control of the timing of cell divisions appears to be widespread in animal tissues (Matsuo et al., 2003), but in adult stem cells this has been demonstrated only rarely (Lucas et al., 2008).

GMC-type neuronal progenitor cells in the proliferation zones divide only once, and this cell cycle is extraordinary long, likely lasting for more than 1 week (Schmidt, 1997, 2001). Hence, adult neurogenesis in the olfactory deuto-cerebrum of decapod crustaceans appears to parallel embryonic and larval neurogenesis of insects in several key aspects: The NSCs maintaining insect embryonic and larval neurogenesis are large NBs that have a short cell cycle, have a high mitotic activity, and divide asymmetrically, whereas GMCs are smaller, divide only once symmetrically, and have a cell cycle that is about twice as long as in NBs (Hartenstein et al., 1987; Egger et al., 2008; Boyan et al., 2010). However, a numerical problem remains in understanding adult neurogenesis in the olfactory deutocerebrum of decapod crustaceans; only one aNB is present per proliferation zone, but according to cell counts at least 10 new PNs per day are produced in each LC (Schmidt, 1997; Sandeman et al., 1998). To generate >10 neurons per day by successive rounds of asymmetric divisions, a single aNB would have to divide asymmetrically at least five times per day, which is not in line with the overall low percentage of mitotic aNBs (Schmidt, 2007a; this study). This numerical discrepancy suggests that an as yet unknown proliferation event is interspersed between the asymmetric aNB divisions and the terminal symmetrical divisions of the GMC-type neuronal progenitor cells. We propose that, in parallel to some embryonic and larval NB lineages of insects (Bello et al., 2008; Boone and Doe, 2008; Bowman et al., 2008; Izergina et al., 2009; Boyan et al., 2010), the differentiating daughters produced by the aNBs act as “transit-amplifying intermediate progenitor cells” and undergo one or more rapid cell divisions through which ultimately the GMC-type neuronal progenitor cells are generated (Fig. 11B). Such rapid cell divisions, which could occur in the center of the proliferation zone containing numerous cells in mitosis ($pH3^+$; Schmidt, 2007a; this study), would have

been missed by in previous BrdU pulse-chase experiments because changes in the number of $BrdU^+$ cells were determined only for survival times >14 hours (Schmidt, 2007a).

Characteristics of the stem cell niche and putative functions of the clump of cells

Densely packed clumps of small cells that form morphologically unique structures in the deutocerebrum were originally described as deutocerebral organs in various species of decapod crustaceans (Bazin and Demeuzy, 1968; Bazin, 1970). Recently, these clumps of cells were identified as part of the neurogenic complexes in the deutocerebrum of *P. argus* (Schmidt, 2007a) and *P. clarkii* (Sullivan et al., 2007a; Song et al., 2009; Zhang et al., 2009). In both species, the clump of cells contains singular proliferating cells, putative aNBs, whose nuclei are significantly larger and more spherical than the nuclei of CFCs. The unique structure of the clumps of cells and their association with the putative NSCs (aNBs) has led to the proposal that they represent stem cell niches (Schmidt, 2007a; Sullivan et al., 2007a; Song et al., 2009). The analysis of the cytoarchitecture and ultra-structure of the clump of cells in the LC of *P. argus* presented here strongly supports this conclusion. First, the clump of cells is composed exclusively of cells of one type—CFCs—which in ultrastructure and labeling with cell-selective markers differ from all other cell types in the olfactory deutocerebrum. Second, the CFCs collectively form a continuous cell layer around the hourglass-shaped aNB and thus are the exclusive constituents of its micro-environment (Fig. 11A). Third, the assemblage of CFCs in turn is ensheathed by a continuous layer of glial processes and thus separated from neurons and arterioles in the surround. Thus, the clump of cells constitutes a unique microenvironment around the aNB. It forms an additional cell layer separating the aNB from surrounding cells that is absent from the neuronal progenitor cells in the proliferation zone, which are in direct membrane contact with each other or with glial cells. With these characteristics, the clump of cells fulfills the morphological criteria of a “protective stem cell niche” as described for many types of continuously replenished tissues of mammals and insects (Spradling et al., 2001; Fuchs et al., 2004; Ohlstein et al., 2004; Moore and Lemischka, 2006; Jones and Wagers, 2008; Morrison and Spradling, 2008).

In spite of its principal correspondence to other stem cell niches in adult tissues, the clump of cells is unique in being composed of only one specific cell type and in forming a morphologically distinct structure. Typically, several cell types participate in the formation of stem cell niches, and, like the stem cells they support, they are dispersed widely throughout the germinal layers of adult tissues (Spradling et al., 2001; Fuchs et al., 2004; Ohlstein et al., 2004; Moore and Lemischka, 2006; Jones and Wagers, 2008; Morrison and Spradling, 2008). This includes the stem cell niches in the subventricular zone of the mammalian brain, which are composed of glial and vascular cells as well as prominent extracellular matrix structures and are widely dispersed throughout the germinal layer (Mercier et al., 2002; Kerever et al., 2007; Shen et al., 2008; Tavazoie et al., 2008). Glial and peri-vascular cells are also closely associated with the clump of cells in the LC of *P. argus* and hence appear to participate in its niche function (Fig. 11A). Extracellular matrix structures, however, were not revealed by TEM, either within the clump of cells or in its immediate surround. The extracellular matrix structure closest to the aNB is the basal lamina overlying the luminal surface of the arteriole that is attached to the clump of cells. Since to be lined by a basal lamina is a constitutive feature of all arterioles, we conclude that most likely extracellular matrix structures are of no particular significance to the cell divisions of aNBs.

The close association of aNBs with clumps of cells in the olfactory deutocerebrum of decapod crustaceans strongly suggests that the clumps of cells have important functions in maintaining aNBs and in supporting their proliferative activity. Generally, a host of

functions is ascribed to stem cell niches, among them 1) nurturing stem cells, 2) shielding stem cells against apoptotic or differentiation stimuli as well as infectious agents, 3) anchoring stem cells, 4) polarizing stem cells to direct their asymmetric divisions, and 5) providing signals for stem cell self-renewal, survival, and maintenance (Spradling et al., 2001; Fuchs et al., 2004; Ohlstein et al., 2004; Moore and Lemischka, 2006; Jones and Wagers, 2008; Morrison and Spradling, 2008). Its peculiar cytoarchitecture and the unique shape of the single aNB within it indicate that some if not all of these functions might be served by the clump of cells.

1. Nurturing the aNB seems a plausible function of the clump of cells, because it is attached to an arteriole through which nutrients and oxygen transported via hemolymph could be delivered. Furthermore, the bulbous foot of the aNB appears to provide an increased area of aNB-CFC cell membrane apposition, which would facilitate transport through this interface. However, our perfusion experiments indicate that hemolymph has no direct access to this interface, and our TEM analysis shows that the arteriole attached to the clump of cells is separated from the CFCs by a continuous and often multilayered sheath of cell body glia processes. Thus, the delivery of nutrients from the hemolymph to the aNB appears to require transport mechanisms in the ensheathing cell body glia and the CFCs. As in *P. argus*, the clump of cells in *P. clarkii* contains a central, nucleus-free area (Song et al., 2009) that was identified as a *vascular cavity* based on perfusion experiments (Sullivan et al., 2007a; Sandeman et al., 2009). Whether it is contiguous with the lumen of neighboring arterioles remains to be determined by TEM.

2. Shielding the aNB against inappropriate signaling molecules and/or infectious agents also appears to be a plausible function of the clump of cells. By forming a thick, continuous cell layer surrounding the aNB, the CFCs constitute a unique cellular barrier between the aNB and other cell types. This extra layer likely makes the aNB less accessible to substances or particles transported in hemolymph than other cells in the LC. Generally, there is no tight blood–brain barrier in the CNS of decapod crustaceans, and relatively large tracer molecules such as ferritin delivered through the hemolymph have access to neurons and glia several micrometers away from arterioles (Abbott, 1972). This is in line with our finding that fluorescent dextrans of 3,000 MW perfused into the cerebral artery labeled extracellular spaces between neuronal somata. That in these experiments the clump of cells remained unlabeled supports the notion that the highly convoluted contours of the CFCs, their thickness, and the tight packing of their processes around the aNB minimize extracellular diffusion. Thus, molecular access to the aNB would be mainly through transport across the CFCs, making them poised to control the flow of molecules to the aNB, either by blocking inappropriate signaling molecules or infectious agents or by facilitating the transport of nutrients or appropriate signaling molecules. The selective labeling of the interface between the CFCs and the bulbous foot of the aNB with several lectins (SBA, HPA, WGA) and anti-Splash suggests that it has a unique molecular composition, which is in line with the assumption that it mediates a highly specialized function, such as the control of molecular exchange between CFCs and the aNB.

3. Anchoring the aNB in the clump of cells is strongly indicated by the unique hourglass-like shape of the aNB. The bulbous foot of the aNB is tightly enclosed by the inner processes of the CFCs, and to retract it from the center of the clump of cells would require extensive morphological rearrangements of these processes. Overall, the hourglass-like shape of the aNB suggests that it consists of two cellular domains with different functions. The bulbous foot seems to be specialized for anchoring the aNB in the clump of cells and for establishing an extensive contact

area with the cell membranes of CFCs. The outer nucleus-contain domain seems to be specialized for producing daughter cells. Through this division of labor, the aNB could undergo repetitive asymmetric divisions without disruption of its anchoring in the clump of cells or its supply by the CFCs.

4. Polarizing the aNB to direct its asymmetric divisions is another plausible function of the clump of cells. The clump of cells is polarized into an apical pole, giving rise to the duct that connects it with the proliferation zone and a basal pole facing in the opposite direction. At the apical pole, the clump of cells gives rise to the duct that connects with the proliferation zone, and it surrounds the nucleus-containing domain of the aNB. This polarization is paralleled by the polarization of the hourglass-shaped aNB into an outer nucleus-containing domain and the inner bulbous foot. As described above, it seems likely that differentiating daughter cells are budded off from the apical pole of the aNB and that they maintain this directionality when they move through the duct toward the proliferation zone. This clear directionality is reminiscent of how in embryonic neurogenesis NBs bud off GMCs strictly at their neuroepithelium-opposing pole and thereby generate columnar cell clones toward the interior of the body (Doe and Goodman, 1985; Hartenstein et al., 1987; Scholtz, 1992). In *Drosophila* the orientation of GMC generation depends on neuroepithelial cells attached to the NB, which itself is not polarized (Siegrist and Doe, 2006). With respect to the orientation of the daughter cells budded off by the aNB, CFCs in *P. argus* have a position equivalent to that of neuroepithelial cells, suggesting that they might be involved in orienting aNB cell divisions. However, the obvious morphological polarization of the aNB leaves open the possibility that orientation of the cell division axis is an intrinsic aNB property.

5. Providing signals for aNB self-renewal, survival, and maintenance may be a function of the clump of cells simply because presumably no such signals can reach the aNB without passing through or being generated by the CFCs. Whether proliferation of aNBs is influenced by signaling molecules has not yet been studied, but, since serotonin and nitric oxide modulate cell divisions in the proliferation zones (Benton et al., 2007; 2008; Sandeman et al., 2009), it is possible that they might also affect the aNB.

Cellular identity of CFCs

One important prerequisite for understanding how the clump of cells functions as a stem cell niche for aNBs is to know the cellular identity of the CFCs. In *P. clarkii*, CFCs were identified as glial cells mainly because they were labeled by anti-GS (Sullivan et al., 2007a,b). Anti-GS is a marker for astrocytes in the mammalian brain (Norenberg, 1979), and it selectively labels a class of glial cells in the brain of decapod crustaceans (Linser et al. 1997; Sullivan et al., 2007a; Harzsch and Hansson, 2008). These GS^+ glial cells have somata at the rim of neuropils, and they extend uni- or multipolar processes into the neuropils, where they branch profusely (Linser et al., 1997). Using the same anti-GS as was used by Sullivan et al. (2007a), we also found distinct and selective labeling of a class of neuropil glia (neuropil glia 1) in the brain of adult *P. argus* with the previously reported morphology. Morphologically these GS^+ glial cells of decapod crustaceans correspond to astrocyte-like neuropil glia identified in insect brains (Oland et al., 1999; Awasaki et al., 2008; Doherty et al., 2009). In our immunocytochemical stainings, anti-GS did not label the CFCs of *P. argus*, and from this we conclude that in *P. argus* the CFCs do not have immunocytochemical properties of neuropil glia 1 cells. Furthermore, the CFCs of *P. argus* differ distinctly from neuropil glia 1 cells in basic cell morphology (CFCs are bipolar; neuropil glia 1 cells are usually mono- or multipolar) and in soma ultrastructure. Since the

CFCs of *P. clarkii* are also bipolar (Sullivan et al., 2007a), their identification as glial cells hinging exclusively on being by anti-GS seems premature (Song et al., 2009). This argument is supported by results of in situ hybridization with a GS-specific probe, which labeled neuropil glia but not the CFCs (Zhang and Beltz, 2010), and by the observation that in the hermit crab, *Coenobita clypeatus*, a structure likely representing the clump of cells is GS^{-}, whereas neuropil glia are GS^{+} (Harzsch and Hansson, 2008, Fig. 5B1).

By TEM and labeling with anti-pH3 and anti-Gs/olf, we identified a distinct class of multipolar cell body glia residing in the LC, MC, and all other neuronal soma clusters. In being multipolar and $pH3^{+}$, cell body glia are clearly distinct from the bipolar and $pH3^{-}$ CFCs, and both cell types differ considerably in ultrastructure. Thus, we conclude that CFCs are not identical to cell body glia. TEM revealed at least three different classes of putative glial cells with somata at the rim of neuropils in addition to putative neuropil glia 1 cells. In their ultrastructural features and multipolar morphology, all of these putative glial cells differ distinctly from CFCs, so we conclude that the CFCs do not correspond to glial cells of these classes.

A previous analysis of cells in the neurogenic complex of *P. argus* based on the measurement of Hoechst-labeled nuclei showed that CFCs are similar to perivascular cells in nuclear size and shape (Schmidt, 2007a). The possibility raised by this result that CFCs may correspond to peri-vascular cells was not corroborated by the more detailed analyses presented here. 1) TEM showed that CFCs and perivascular cells differ distinctly in electron density and organelle composition of the cytoplasm as well as in nuclear ultrastructure. 2) TEM also demonstrated that a basal lamina covers the entire luminal surface of perivascular cells but is not present on the surface of CFCs or anywhere else in the clump of cells. 3) ACL intensely labeled perivascular cells, including those of the arteriole attached to the clump of cells, but failed to label CFCs. 4) Conversely, anti-Gs/olf intensely labeled cell membranes of CFCs but failed to label arterioles. Collectively, these results strongly support the notion that CFCs do not represent perivascular cells.

Besides glial and perivascular cells, neurons are the main cell type present in the olfactory deutocerebrum. CFCs are clearly different from neurons in basic morphology (small bipolar vs. large unipolar) as well as in the ultrastructure of cytoplasm and nucleus. Both cell types are also distinctly different in labeling by cell-type-selective probes: neurons are WGA^{+} and ACL^{+} but anti-Gs/ olf^{-}, whereas the opposite is true for CFCs. Thus, we conclude that CFCs are not neurons.

In conclusion, our results fail to provide evidence that in *P. argus* the CFCs correspond to any of the cell types that can be identified in the olfactory deutocerebrum composed of several types of glia, perivascular cells, and neurons. Thus, CFCs appear to represent a different, as yet unidentified cell type, and we propose that they might correspond to embryonic neuroepithelial cells. This hypothesis is based on the observation that, after delamination from the neuroepithelium, embryonic NBs of insects remain associated with elongated processes of neuroepithelial cells (also called *sheath cells*), which, like CFCs, have distinct bipolar morphology (Doe and Goodman, 1985). The CFCs/aNB association and the sheath cells/embryonic NB association have a similar morphological polarization in that, in both cases, the differentiating NB daughters are generated at the pole of the NB opposite where the somata of CFCs or sheath cells are located. In embryonic neurogenesis, this polarization results in the production of neurons into the interior of the body, and a corresponding directionality is maintained in adult neurogenesis, when new neurons are produced at more internal locations of the brain (proliferation zones) than positions occupied by the aNB. This new hypothesis about the cellular identity of the CFCs implies that the

stem cell niche provided by the clump of cells primarily maintains a microenvironment for the aNB with features of the embryonic neuroepithelium.

Conclusions: Cellular basis of adult neurogenesis across animal taxa

The results of this study allow a more detailed comparison of the cellular basis of adult neurogenesis among the three bilaterian taxa in which new neurons are continuously generated in select brain regions of adults: decapod crustaceans, insects, and vertebrates, in particular mammals (Lindsey and Tropepe, 2006; Fig. 12). Adult neurogenesis in decapod crustaceans shows important commonalities with adult neurogenesis in insects with respect to the identity of the NSCs and the cell lineages to which they give rise. In both taxa, the NSCs maintaining adult neurogenesis are represented by a few large NBs of invariant location within or close to the neuronal soma clusters in which new neurons are generated (Figs. 11B, 12B,D). Through successive asymmetric divisions, the aNBs ultimately give rise to neuronal progenitor cells (GMCs) that undergo one terminal symmetrical division producing two neurons. We speculate that, in decapod crustaceans, at least some daughter cells generated by the aNBs act as transit-amplifying intermediate progenitor cells providing a mechanism to produce the high number of neuronal progenitor cells associated with each aNB. Transit-amplifying intermediate progenitor cells have been documented in some embryonic and larval NB lineages of insect brains (see above) but not in NB lineages producing the Kenyon cells of the mushroom bodies (Bello et al., 2008; Boyan et al., 2010), the only neurons that continue to be generated in the brain of adult insects (Cayre et al., 2002). Thus, it seems unlikely that transit-amplifying intermediate progenitor cells contribute to adult neurogenesis in the brain of insects. A substantial difference between adult neurogenesis in decapod crustaceans and insects is that, in decapod crustaceans, but not in insects, aNBs are associated with clumps of cells likely representing stem cell niches. Based on the finding that, in *Drosophila*, glial cells associated with larval NBs secrete glycoproteins regulating NB proliferation (Ebens et al., 1993), it has been suggested that these glial cells form a stem cell niche for late embryonic and larval NBs (Maurange and Gould, 2005). However, glial cells are not associated with the neuronal progenitor cells in the Kenyon cell layer of adult crickets in a pattern suggesting that they form a stem cell niche (Mashaly et al., 2008). We hypothesize that the presence or lack of a stem cell niche associated with the aNBs reflects the generally enormous difference in the duration of adult neurogenesis between decapod crustaceans and insects. In decapod crustaceans, adult neurogenesis persists throughout the entire adult life span, which for most species (including *P. argus* and *P. clarkii*) ranges from years to decades (Farmer, 1973; Lyons et al., 1981; Belchier et al., 1998; Sheehy et al., 1999; Maxwell et al., 2007). In contrast, insect species with adult neurogenesis have an adult life span is in the range of months and adult neurogenesis ceases within the first weeks of adult life (Gu et al., 1999; Zhao et al., 2008). Thus, adult neurogenesis in insects can be interpreted as a transient continuation of larval/pupal neurogenesis that is enabled simply by preventing apoptotic cell death of the mushroom body NBs (Siegrist et al., 2010). In contrast, adult neurogenesis in decapod crustaceans is a much more prolonged process and as such appears to require that a stem cell niche provide additional support for the aNBs to sustain their long-term survival and proliferative potential.

Adult neurogenesis in decapod crustaceans and insects appears to differ fundamentally from adult neurogenesis in mammals with respect to the identity, number, and proliferation dynamics of the NSCs maintaining it. In decapod crustaceans and insects, the NSCs maintaining adult neurogenesis are infrequent, tetraconate-typical NBs, characterized by being large, by not having a differentiated cell phenotype (neither neuronal nor glial cell morphology), and by lacking a primary cilium. In contrast, the NSCs maintaining adult neurogenesis in mammals have a glial cell (astrocytic) phenotype, bear a primary cilium,

and are dispersed throughout extensive germinal layers, the subventricular zone of the lateral ventricles, and the subgranular region of the hippocampus (Kriegstein and Alvarez-Buylla, 2009; Fig. 12F). The aNBs of decapod crustaceans and insects appear to be actively proliferating, insofar as they are readily labeled by single BrdU applications (Dufour and Gadenne, 2006; Zhao et al., 2008; Song et al., 2009; this study), whereas NSCs of mammals are labeled only after extended exposure to BrdU and thus are largely quiescent (Doetsch et al., 1999a,b).

In spite of these substantial differences in the nature of the NSCs, adult neurogenesis in decapod crustaceans (but not in insects; see above) parallels adult neurogenesis in mammals in several ways. First, adult neurogenesis is maintained throughout the entire adult life, which in decapod crustaceans (see above) as well as in mammals lasts for several years to decades (De Magalahaes and Costa, 2009). Second, both taxa have an age-dependent decrease in proliferative activity (Kuhn et al., 1996; Hansen and Schmidt, 2004; Luo et al., 2006). Third, both taxa have stem cell niches supporting the NSCs. Likely these common features of adult neurogenesis in decapod crustaceans and mammals are causally linked in that stem cell niches are required for the long-term preservation of NSCs but cannot completely prevent their “aging.”

In conclusion, adult neurogenesis in the brain shows a very basic similarity among crustaceans, insects, and mammals, in that in each taxon the NSCs maintaining adult neurogenesis have the same identity as those fueling embryonic (and if present larval) neurogenesis. Thus, adult neurogenesis can be viewed as a prolonged extension of embryonic neurogenesis. Furthermore, the presence of stem cell niches associated with the NSCs fueling adult neurogenesis in decapod crustaceans and mammals, but not in insects, suggests that NSC niches are a prerequisite for preserving the NSC proliferative activity for years or even decades of adult life. To understand the principle mechanisms by which this impressive feat is achieved by neural stem cell niches, it will be informative to compare those of decapod crustaceans and mammals, especially because their NSCs are of different cellular identity and their niches are of different cellular composition. The fact that, in decapod crustacean brains, the NSCs (=aNBs) and their stem cell niches (=clumps of cells) are morphologically identifiable makes them uniquely amenable for analyzing their cellular and physiological interactions.

Acknowledgments

Grant sponsor: National Institutes of Health; Grant number: DC00312.

We thank Vu Ngo for help with animal care and Vivian Ngo-Vu for excellent assistance with immunocytochemistry. We also thank the Developmental Studies Hybridoma Bank for providing antisynapsin antibody.

Abbreviations

ACL	*Amaranthus caudatus* lectin
AL	accessory lobe
aNB	adult neuroblast
anti-GS	anti-glutamine synthetase
anti-Gs/olf	anti-Gas/olf
anti-pH$_3$	anti-phospho-histone H$_3$ [Ser 10]
anti-Splash	anti-Spiny lobster achaete scute homolog

anti-Syn	anti-Synapsin
BrdU	5-bromo-2′-deoxyuridine
CFC	clump-forming cell
GMC	ganglion mother cell
HPA	*Helix pomatia* agglutinin
LC	lateral soma cluster
LN	local interneuron
MC	medial soma cluster
NB	neuroblast
NSC	neural stem cell
OL	olfactory lobe
PN	projection neuron
SBA	Soy bean agglutinin
SPB	Sörensen phosphate buffer
TEM	transmission electron microscopy
WGA	Wheat germ agglutinin

LITERATURE CITED

Abbott NJ. The organization of the cerebral ganglion in the shore crab, *Carcinus maenas*. II. The relation of intra-cerebral blood vessels to other brain elements. Z Zellforsch. 1971; 120:401–419. [PubMed: 5151348]

Abbott NJ. Access of ferritin to the interstitial space of *Carcinus* brain from intracerebral blood vessels. Tissue & Cell. 1972; 4:99–104. [PubMed: 4647366]

Alvarez-Buylla A, García-Verdugo JM, Mateo AS, Merchant-Larios H. Primary neural precursors and intermitotic nuclear migration in the ventricular zone of adult canaries. J Neurosci. 1998; 18:1020–1037. [PubMed: 9437023]

Alvarez-Buylla A, García-Verdugo JM, Tramontin AD. A unified hypothesis on the lineage of neural stem cells. Nat Rev Neurosci. 2001; 2:287–293. [PubMed: 11283751]

Awasaki T, Lai S-L, Ito K, Lee T. Organization and post-embryonic development of glial cells in the adult central brain of *Drosophila*. J Neurosci. 2008; 28:13742–13753. [PubMed: 19091965]

Bazin F. Étude comparée de l'organe deutocerebral des Macroures Reptantia et des Anomures (Crustacés Décapodes). Arch Zool Exp Gen. 1970; 111:245–264.

Bazin F, Demeuzy N. Existence d'organes intracéré-braux énigmatiques chez le Crustacé Décapode *Carcinus maenas* (L.). C R Acad Sci. 1968; 267:356–358.

Belchier M, Edsman L, Sheehy MRJ, Shelton PMJ. Estimating age and growth in long-lived temperate freshwater crayfish using lipofuscin. Freshwater Biol. 1998; 39:439–446.

Bello BC, Izergina N, Caussinus E, Reichert H. Amplification of neural stem cell proliferation by intermediate progenitor cells in *Drosophila* brain development. Neural Dev. 2008; 3:5. [PubMed: 18284664]

Benton JL, Sandeman DC, Beltz BS. Nitric oxide in the crustacean brain: regulation of neurogenesis and morphogenesis in the developing olfactory pathway. Dev Dyn. 2007; 236:3047–3060. [PubMed: 17948307]

Benton JL, Goergen EM, Rogan SC, Beltz BS. Hormonal and synaptic influences of serotonin on adult neurogenesis. Gen Comp Endocrinol. 2008; 158:183–190. [PubMed: 18692503]

Boone JQ, Doe CQ. Identification of *Drosophila* type II neuroblast lineages containing transit amplifying ganglion mother cells. Dev Neurobiol. 2008; 68:1185–1195. [PubMed: 18548484]

Bowman SK, Rolland V, Betschinger J, Kinsey KA, Emery G, Knoblich JA. The tumor suppressors Brat and Numb regulate transit-amplifying neuroblast lineages in *Drosophila*. Dev Cell. 2008; 14:535–546. [PubMed: 18342578]

Boyan G, Williams L, Legl A, Herbert Z. Proliferative cell types in embryonic lineages of the central complex of the grasshopper *Schistocerca gregaria*. Cell Tissue Res. 2010; 341:259–277. [PubMed: 20571828]

Breunig JJ, Sarkisian MR, Arellano JI, Morozov YM, Ayoub AE, Sojitra S, Wang B, Flavell RA, Rakic P, Town T. Primary cilia regulate hippocampal neurogenesis by mediating sonic hedgehog signaling. Proc Natl Acad Sci U S A. 2008; 105:13127–13132. [PubMed: 18728187]

Cayre M, Strambi C, Strambi A. Neurogenesis in an adult insect brain and its hormonal control. Nature. 1994; 368:57–59.

Cayre M, Strambi C, Charpin P, Augier R, Meyer MR, Edwards JS, Strambi A. Neurogenesis in adult insect mushroom bodies. J Comp Neurol. 1996; 371:300–310. [PubMed: 8835734]

Cayre M, Malaterre J, Scotto-Lomassese S, Strambi C, Strambi A. The common properties of neurogenesis in the adult brain: from invertebrates to vertebrates. Comp Biochem Physiol B. 2002; 132:1–15. [PubMed: 11997205]

Chien H, Tadesse T, Liu H, Schmidt M, Walthall WW, Tai PC, Derby CD. Molecular cloning and characterization of homologs of *achaetescute* and *hairy-enhancer of split* in the olfactory organ of the spiny lobster *Panulirus argus*. J Mol Neurosci. 2009; 39:294–307. [PubMed: 19322682]

De Magalhaes JP, Costa J. A database of vertebrate longevity records and their relation to other life-history traits. J Evol Biol. 2009; 22:1770–1774. [PubMed: 19522730]

Doe CQ. Neural stem cells: balancing self-renewal with differentiation. Development. 2008; 135:1575–1587. [PubMed: 18356248]

Doe CQ, Goodman CS. Early events in insect neurogenesis. I. Development and segmental differences in the pattern of neuronal precursor cells. Dev Biol. 1985; 111:193–205. [PubMed: 4029506]

Doe CQ, Fuerstenberg S, Peng CY. Neural stem cells: from fly to vertebrates. J Neurobiol. 1998; 36:111–127. [PubMed: 9712299]

Doetsch F, Caillé I, Lim DA, García-Verdugo JM, Alvarez-Buylla A. Subventricular zone astrocytes are neural stem cells in the adult mammalian brain. Cell. 1999a; 97:703–716. [PubMed: 10380923]

Doetsch F, García-Verdugo JM, Alvarez-Buylla A. Regeneration of a germinal layer in the adult mammalian brain. Proc Natl Acad Sci U S A. 1999b; 96:11619–11624. [PubMed: 10500226]

Doherty J, Logan MA, Tasdemir OE, Freeman MR. Ensheathing glia function as phagocytes in the adult *Drosophila* brain. J Neurosci. 2009; 29:4768–4781. [PubMed: 19369546]

Dohle W. Die Bildung und Differenzierung des postnauplialen Keimstreifs von *Diastylis rathkei* (Crustacea, Cumacea). II. Die Differenzierung und Musterbildung des Ektoderms. Zoomorphologie. 1976; 84:235–277.

Dohle W. Are the insects terrestrial crustaceans? A discussion of some new facts and arguments and the proposal of the proper name “Tetraconata” for the monophyletic unit Crustacea + Hexapoda. Ann Soc Entomol Fr. 2001; 37:85–103.

Dufour M-C, Gadenne C. Adult neurogenesis in a moth brain. J Comp Neurol. 2006; 495:635–643. [PubMed: 16498684]

Ebens AJ, Garren H, Cheyette BNR, Zipursky SL. The *Drosophila* anachronism locus: a glycoprotein secretet by glia inhibits neuroblast proliferation. Cell. 1993; 74:15–27. [PubMed: 7916657]

Egger B, Chell JM, Brand AH. Insights into neural stem cell biology from flies. Philos Trans R Soc Lond B Biol Sci. 2008; 363:39–56. [PubMed: 17309865]

Eisenberg D, Gill HS, Pfluegl GMU, Rotstein SH. Structure–function relationships of glutamine synthetases. Biochim Biophys Acta. 2000; 1477:122–145. [PubMed: 10708854]

Farmer AS. Age and growth in *Nephrops norvegicus* (Decapoda: Nephropidae). Mar Biol. 1973; 23:315–325.

Fuchs E. The tortoise and the hair: slow-cycling cells in the stem cell race. Cell. 2009; 137:811–819. [PubMed: 19490891]

Fuchs E, Tumbar T, Guasch G. Socializing with neighbors: stem cells and their niche. Cell. 2004; 116:769–778. [PubMed: 15035980]

Ghosal K, Gupta M, Killian KA. Agonistic behavior enhances adult neurogenesis in male *Acheta domesticus* crickets. J Exp Biol. 2009; 212:2045–2056. [PubMed: 19525431]

Gu SH, Tsia WH, Chiang AS, Chow YS. Mitogenic effects of 20-hydroxyecdysone on neurogenesis in adult mushroom bodies of the cockroach, *Diploptera punctata*. J Neurobiol. 1999; 39:264–274. [PubMed: 10235680]

Han Y-G, Spassky N, Romaguera-Ros M, García-Verdugo JM, Aguilar A, Schneider-Maunoury S, Alvarez-Buylla A. Hedgehog signaling and primary cilia are required for the formation of adult neural stem cells. Nat Neurosci. 2008; 11:277–284. [PubMed: 18297065]

Hansen A, Schmidt M. Neurogenesis in the central olfactory pathway of the adult shore crab *Carcinus maenas* is controlled by sensory afferents. J Comp Neurol. 2001; 441:223–233. [PubMed: 11745646]

Hansen A, Schmidt M. Influence of season and environment on adult neurogenesis in the central olfactory pathway of the shore crab, *Carcinus maenas*. Brain Res. 2004; 1025:85–97. [PubMed: 15464748]

Hartenstein V, Rudloff E, Campos-Ortega JA. The pattern of proliferation of the neuroblasts in the wild-type embryo of *Drosophila melanogaster*. Roux's Arch Dev Biol. 1987; 196:473–485.

Harzsch S. Neurogenesis in the crustacean ventral nerve cord: homology of neuronal stem cells in Malacostraca and Branchiopoda? Evol Dev. 2001; 3:154–169. [PubMed: 11440250]

Harzsch S, Hansson BS. Brain architechture in the terrestrial hermit crab *Coenobita clypeatus* (Anomura, Coenobitidae), a crustacean with good aerial sense of smell. BMC Neurosci. 2008; 9:58. [PubMed: 18590553]

Harzsch S, Anger K, Dawirs RR. Immunocytochemical detection of acetylated α-tubulin and *Drosophila* synapsin in the embryonic crustacean nervous system. Int J Dev Biol. 1997; 41:477–484. [PubMed: 9240564]

Harzsch S, Miller J, Benton J, Dawirs RR, Beltz B. Neurogenesis in the thoracic neuromeres of two crustaceans with different types of metamorphic development. J Exp Biol. 1998; 201:2465–2479. [PubMed: 9698581]

Harzsch S, Miller J, Benton J, Beltz B. From embryo to adult: persistent neurogenesis and apoptotic cell death shape the lobster deutocerebrum. J Neurosci. 1999; 19:3472–3485. [PubMed: 10212307]

He S, Nakada D, Morrison SJ. Mechanisms of stem cell self-renewal. Annu Rev Cell Dev Biol. 2009; 25:377–406. [PubMed: 19575646]

Hendzel MJ, Wei Y, Mancini MA, Van Hooser A, Ranalli T, Brinkley BR, Bazett-Jones DP, Allis CD. Mitosis-specific phosphorylation of histone H3 initiates primarily within pericentromeric heterochromatin during G2 and spreads in an ordered fashion coincident with mitotic chromosome condensation. Chromosoma. 1997; 106:348–360. [PubMed: 9362543]

Hertz L, Dringen R, Schousboe A, Robinson SR. Astrocytes: glutamate producers for neurons. J Neurosci Res. 1999; 57:417–428. [PubMed: 10440891]

Hose JE, Martin GG, Gerard AS. A decapod hemocyte classification scheme integrating morphology, cytochemistry, and function. Biol Bull. 1990; 178:33–45.

Hoyle G. Glial cells of an insect ganglion. J Comp Neurol. 1986; 246:85–103. [PubMed: 3700719]

Izergina N, Balmer J, Bello B, Reichert H. Postembryonic development of transit amplifying neuroblast lineages in the *Drosophila* brain. Neural Dev. 2009; 4:44. [PubMed: 20003348]

Jacobs K, Lakes-Harlan R. Lectin histochemistry of the metathoracic ganglion of the locust *Schistocerca gregaria* before and after axotomy of the tympanal nerve. J Comp Neurol. 1997; 387:255–265. [PubMed: 9336227]

Jones DL, Wagers AJ. No place like home: anatomy and function of the stem cell niche. Nat Rev Mol Cell Biol. 2008; 9:11–21. [PubMed: 18097443]

Kerever A, Schnack J, Vellinga D, Ichikawa N, Moon C, Arikawa-Hirasawa E, Efird JT, Mercier F. Novel extracellular matrix structures in the neural stem cell niche capture the neurogenic factor

fibroblast growth factor 2 from the extracellular milieu. Stem Cells. 2007; 25:2146–2157. [PubMed: 17569787]

Klagges BRE, Heimbeck G, Godenschwege TA, Hofbauer A, Pflugfelder GO, Reifegerste R, Reisch D, Schaupp M, Buchner S, Buchner E. Invertebrate synapsins: a single gene codes for several isoforms in *Drosophila*. J Neurosci. 1996; 16:3154–3165. [PubMed: 8627354]

Krajewski WW, Collins R, Holmberg-Schiavone L, Jones TA, Karlberg T, Mowbray SL. Crystal structures of mammalian glutamine synthetases illustrate substrate-induced conformational changes and provide opportunities for drug and herbicide design. J Mol Biol. 2008; 375:217–228. [PubMed: 18005987]

Kriegstein A, Alvarez-Buylla A. The glial nature of embryonic and adult neural stem cells. Annu Rev Neurosci. 2009; 32:149–184. [PubMed: 19555289]

Kuhn HG, Dickinson-Anson H, Gage FH. Neurogenesis in the dentate gyrus of the adult rat: Age-related decrease of neuronal progenitor proliferation. J Neurosci. 1996; 16:2027–2033. [PubMed: 8604047]

Li L, Clevers H. Coexistence of quiescent and active adult stem cells in mammals. Science. 2010; 327:542–545. [PubMed: 20110496]

Lindsey BW, Tropepe V. A comparative framework for understanding the biological principles of adult neurogenesis. Prog Neurobiol. 2006; 80:281–307. [PubMed: 17218052]

Linser PJ, Trapido-Rosenthal HG, Orona E. Glutamine synthetase is a glial-specific marker in the olfactory regions of the lobster (*Panulirus argus*) nervous system. Glia. 1997; 20:275–283. [PubMed: 9262232]

Lucas D, Battista M, Shi PA, Isola L, Frenette PS. Mobilized hematopoietic stem cell yield depends on species-specific circadian timing. Cell Stem Cell. 2008; 3:364–366. [PubMed: 18940728]

Luo J, Daniels SB, Lennington JB, Notti RQ, Conover JC. The aging neurogenic subventricular zone. Aging Cell. 2006; 5:139–152. [PubMed: 16626393]

Lyons WG, Barber DG, Foster SM, Kennedy FS jr, Milano GR. The spiny lobster, *Panulirus argus*. Middle and Upper Florida Keys: population structure, structure dynamics, and reproduction. Florida Mar Res Publ. 1981; 38:1–38.

Mashaly A, Winkler M, Frambach I, Gras H, Schürmann F-W. Sprouting interneurons in mushroom bodies of adult cricket brains. J Comp Neurol. 2008; 508:153–174. [PubMed: 18306378]

Matsuo T, Yamaguchi S, Mitsui S, Emi A, Shimoda F, Okamura H. Control mechanism of the circadian clock for timing of cell division in vivo. Science. 2003; 302:255–259. [PubMed: 12934012]

Maurange C, Gould AP. Brainy but not too brainy: starting and stopping neuroblast divisions in *Drosophila*. Trends Neurosci. 2005; 28:30–36. [PubMed: 15626494]

Maxwell KE, Matthews TR, Sheehy MRJ, Bertelsen RD, Derby CD. Neurolipofuscin is a measure of age in *Panulirus argus*, the Caribbean spiny lobster, in Florida. Biol Bull. 2007; 213:55–66. [PubMed: 17679720]

McKinnon E, Hargittai PT, Grossfeld RM, Lieberman EM. Glutamine cycle enzymes in the crayfish giant nerve fiber: implications for axon-to-glia signaling. Glia. 1995; 14:198–208. [PubMed: 7591031]

Mercier F, Kitasako JT, Hatton GI. Anatomy of the brain neurogenic zones revisited: fractones and the fibroblast/ macrophage network. J Comp Neurol. 2002; 451:170–188. [PubMed: 12209835]

Merkle FT, Tramontin AD, García-Verdugo JM, Alvarez-Buylla A. Radial glia give rise to adult neural stem cells in the sub-ventricular zone. Proc Natl Acad Sci U S A. 2004; 101:17528–17532. [PubMed: 15574494]

Mirzadeh Z, Merkle FT, Soriano-Navarro M, García-Verdugo JM, Alvarez-Buylla A. Neural stem cells confer unique pinwheel architecture to the ventricular surface in neurogenic regions of the adult brain. Cell Stem Cell. 2008; 3:265–278. [PubMed: 18786414]

Moore KA, Lemischka IR. Stem cells and their niches. Science. 2006; 311:1880–1885. [PubMed: 16574858]

Morrison SJ, Spradling AC. Stem cells and niches: mechanisms that promote stem cell maintenance throughout life. Cell. 2008; 132:598–611. [PubMed: 18295578]

Morshead CM, Reynolds BA, Craig CG, McBurney MW, Staines WA, Morassutti D, Weiss S, Van der Kooy D. Neural stem cells in the adult mammalian forebrain: a relatively quiescent subpopulation of subependymal cells. Neuron. 1994; 13:1071–1082. [PubMed: 7946346]

Norenberg MD. The distribution of glutamine synthetase in the rat central nervous system. J Histochem Cytochem. 1979; 27:756–762. [PubMed: 39099]

Ohlstein B, Kai T, Decotto E, Spradling A. The stem cell niche: theme and variations. Curr Opin Cell Biol. 2004; 16:693–699. [PubMed: 15530783]

Oland LA, Marrero HG, Burger I. Glial cells in the developing and adult olfactory lobe of the moth *Manduca sexta*. Cell Tissue Res. 1999; 297:527–545. [PubMed: 10460499]

Orona E, Battelle B-A, Ache BW. Immunohistochemical and biochemical evidence for the putative inhibitory neuro-transmitters histamine and GABA in lobster olfactory lobes. J Comp Neurol. 1990; 294:633–646. [PubMed: 2341629]

Palmer TD, Willhoite AR, Gage FH. Vascular niche for adult hippocampal neurogenesis. J Comp Neurol. 2000; 425:479–494. [PubMed: 10975875]

Quan F, Forte MA. Two forms of *Drosophila melanogaster* Gsα are produced by alternate splicing involving an unusual splice site. Mol Cell Biol. 1990; 10:910–917. [PubMed: 2106072]

Regier JC, Shultz JW, Zwick A, Hussey A, Ball B, Wetzer R, Martin JW, Cunningham CW. Arthropod relationships revealed by phylogenomic analysis of nuclear protein-coding sequences. Nature. 2010; 463:1079–1083. [PubMed: 20147900]

Sandeman DC. The vascular circulation in the brain, optic lobes and thoracic ganglia of the crab *Carcinus*. Proc R Soc Lond B Biol Sci. 1967; 168:82–90. [PubMed: 4382873]

Sandeman D, Sandeman R, Derby C, Schmidt M. Morphology of the brain of crayfish, crabs, and spiny lobsters: a common nomenclature for homologous structures. Biol Bull. 1992; 183:304–326.

Sandeman DC, Luff SE. The structural organization of glomerular neuropile in the olfactory and accessory lobes of an Australian freshwater crayfish, *Cherax destructor*. Z Zellforsch. 1973; 142:37–61. [PubMed: 4356034]

Sandeman DC, Benton JL, Beltz BS. An identified serotonergic neuron regulates adult neurogenesis in the crustacean brain. Dev Neurobiol. 2009; 69:530–545. [PubMed: 19373861]

Sandeman R, Clarke D, Sandeman D, Manly M. Growth-related and antennular amputation-induced changes in the olfactory centers of crayfish brain. J Neurosci. 1998; 18:6195–6206. [PubMed: 9698313]

Schachtner J, Schmidt M, Homberg U. Organization and evolutionary trends of primary olfactory brain centers in Tetraconata (Crustacea + Hexapoda). Arthrop Struct Dev. 2005; 34:257–299.

Schmidt M. Continuous neurogenesis in the olfactory brain of adult shore crabs, *Carcinus maenas*. Brain Res. 1997; 762:131–143. [PubMed: 9262167]

Schmidt M. Neuronal differentiation and long-term survival of newly generated cells in the olfactory midbrain of the adult spiny lobster, *Panulirus argus*. J Neurobiol. 2001; 48:181–203. [PubMed: 11466706]

Schmidt M. Identification of putative neuroblasts at the base of adult neurogenesis in the olfactory midbrain of the spiny lobster, *Panulirus argus*. J Comp Neurol. 2007a; 503:64–84. [PubMed: 17480012]

Schmidt M. The olfactory pathway of decapod crustaceans—an invertebrate model for life-long neurogenesis. Chem Senses. 2007b; 32:365–384. [PubMed: 17404151]

Schmidt M, Ache BW. Descending neurons with dopamine-like or with substance P/FMRF-like immunoreactivity target the somata of olfactory interneurons in the brain of the spiny lobster, *Panulirus argus*. Cell Tissue Res. 1994; 278:337–352. [PubMed: 7528099]

Schmidt M, Ache BW. Processing of antennular input in the brain of the spiny lobster, *Panulirus argus*. II. The olfactory pathway. J Comp Physiol A. 1996; 178:605–628.

Schmidt M, Ache BW. Immunocytochemical analysis of glomerular regionalization and neuronal diversity in the olfactory deutocerebrum of the spiny lobster. Cell Tissue Res. 1997; 287:541–563. [PubMed: 9027299]

Schmidt M, Harzsch S. Comparative analysis of neurogenesis in the central olfactory pathway of adult decapod crustaceans by in vivo BrdU labeling. Biol Bull. 1999; 196:127–136.

Scholtz G. Cell lineage studies in the crayfish *Cherax destructor* (Crustacea, Decapoda): germ band formation, segmentation, and early neurogenesis. Roux Arch Dev Biol. 1992; 202:36–48.

Sheehy MRJ, Bannister RCA, Wickins JF, Shelton PMJ. New perspectives on the growth and longevity of the European lobster (*Homarus gammarus*). Can J Fish Aquat Sci. 1999; 56:1904–1915.

Shen Q, Wang Y, Kokovay E, Lin G, Chuang S-M, Goderie SK, Roysam B, Temple S. Adult SVZ stem cells lie in a vascular niche: a quantitative analysis of niche cell–cell interactions. Cell Stem Cell. 2008; 3:289–300. [PubMed: 18786416]

Siegrist SE, Doe CQ. Extrinsic cues orient the cell division axis in *Drosophila* embryonic neuroblasts. Development. 2006; 133:529–536. [PubMed: 16396904]

Siegrist SE, Haque NS, Chen C-H, Hay BA, Hariharan IK. Inactivation of both *foxo* and *reaper* promotes long-term adult neurogenesis in *Drosophila*. Curr Biol. 2010; 20:643–648. [PubMed: 20346676]

Song C-K, Johnstone LM, Edwards DH, Derby CD, Schmidt M. Cellular basis of neurogenesis in the brain of crayfish, *Procambarus clarkii*: neurogenic complex in the olfactory midbrain from hatchlings to adults. Arthrop Struct Dev. 2009; 38:339–360.

Spradling A, Drummond-Barbosa D, Kai T. Stem cells find their niche. Nature. 2001; 414:98–104. [PubMed: 11689954]

Strausfeld NJ, Sinakevitch I, Brown SM, Farris SM. Ground plan of the insect mushroom body: functional and evolutionary implications. J Comp Neurol. 2009; 513:265–291. [PubMed: 19152379]

Sullivan JM, Beltz BS. Neural pathways connecting the deutocerebrum and lateral protocerebrum in the brains of decapod crustaceans. J Comp Neurol. 2001; 441:9–22. [PubMed: 11745632]

Sullivan JM, Beltz BS. Adult neurogenesis in the central olfactory pathway in the absence of receptor neuron turnover in *Libinia emarginata*. Eur J Neurosci. 2005a; 22:2397–2405. [PubMed: 16307582]

Sullivan JM, Beltz BS. Newborn cells in the adult crayfish brain differentiate into distinct neuronal types. J Neurobiol. 2005b; 65:157–170. [PubMed: 16114027]

Sullivan JM, Benton JL, Sandeman DC, Beltz BS. Adult neurogenesis: a common strategy across diverse species. J Comp Neurol. 2007a; 500:574–584. [PubMed: 17120293]

Sullivan JM, Sandeman DC, Benton JL, Beltz BS. Adult neurogenesis and cell cycle regulation in the crustacean olfactory pathway: from glial precursors to differentiated neurons. J Mol Histol. 2007b; 38:527–542. [PubMed: 17624620]

Tang X, Falls DL, Li X, Lane T, Luskin MB. Antigen-retrieval procedure for bromodeoxyuridine immunolabeling with concurrent labeling of nuclear DNA and antigens damaged by HCl pretreatment. J Neurosci. 2007; 27:5837–5844. [PubMed: 17537952]

Tavazoie M, Van der Veken L, Silva-Vargas V, Louissaint M, Colonna L, Zaidi B, García-Verdugo JM, Doetsch F. A specialized vascular niche for adult neural stem cells. Cell Stem Cell. 2008; 3:279–288. [PubMed: 18786415]

Telford MJ, Bourlat SJ, Economou A, Papillon D, Rota-Stabelli O. The evolution of the Ecdysozoa. Philos Trans R Soc Lond B Biol Sci. 2008; 363:1529–1537. [PubMed: 18192181]

Trapido-Rosenthal HG, Linser PJ, Greenberg RM, Gleeson RA, Carr WES. cDNA clones from the olfactory organ of the spiny lobster encode a protein related to eukaryotic glutamine synthetase. Gene. 1993; 129:275–278. [PubMed: 8100791]

Ungerer P, Scholtz G. Filling the gap between identified neuroblasts and neurons in crustaceans adds new support for Tetraconata. Proc R Soc Lond B Biol Sci. 2008; 275:369–376.

Urbach R, Technau GM. Early steps in building the insect brain: neuroblast formation and segmental patterning in the developing brain of different insect species. Arthrop Struct Dev. 2003; 32:103–123.

Wachowiak M, Ache BW. Morphology and physiology of multiglomerular olfactory projection neurons in the spiny lobster. J Comp Physiol A. 1994; 175:35–48.

Wachowiak M, Ache BW. Dual inhibitory pathways mediated by GABA- and histaminergic interneurons in the lobster olfactory lobe. J Comp Physiol A. 1997; 180:357–372.

Wachowiak M, Diebel CE, Ache BW. Functional organization of olfactory processing in the accessory lobe of the spiny lobster. J Comp Physiol A. 1996; 178:211–226.

Wei Y, Mizzen CA, Cook RG, Gorovsky MA, Allis CD. Phosphorylation of histone H3 at serine 10 is correlated with chromosome condensation during mitosis and meiosis in *Tetrahymena*. Proc Natl Acad Sci U S A. 1998; 95:7480–7484. [PubMed: 9636175]

Xu F, Hollins B, Gress AM, Landers TM, McClintock TS. Molecular cloning and characterization of a lobster Gαs protein expressed in neurons of olfactory organ and brain. J Neurochem. 1997; 69:1793–1800. [PubMed: 9349521]

Yasugi T, Umetsu D, Murakami S, Sato M, Tabata T. *Drosophila* optic lobe neuroblasts triggered by a wave of proneural gene expression that is negatively regulated by JAK/STAT. Development. 2008; 135:1471–1480. [PubMed: 18339672]

Ye W, Mairet-Coello G, DiCicco-Bloom E. DNAse I pre-treatment markedly enhances detection of nuclear cyclin-dependent kinase inhibitor p57Kip2 and BrdU double immunostaining in embryonic rat brain. Histochem Cell Biol. 2007; 127:195–203. [PubMed: 17024454]

Zhang, Y.; Beltz, BS. 2010 Neuroscience Meeting Planner. San Diego, CA: Society for Neuroscience; 2010. Glutamine sythetase, a functionally active enzyme in the crayfish brain. Program No. 737.14

Zhang Y, Allodi S, Sandeman DC, Beltz BS. Adult neurogenesis in the crayfish brain: proliferation, migration, and possible origin of precursor cells. Dev Neurobiol. 2009; 69:415–436. [PubMed: 19294644]

Zhao X, Coptis V, Farris SM. Metamorphosis and adult development of the mushroom bodies of the red flour beetle, *Tribolium castaneum*. Dev Neurobiol. 2008; 68:1487–1502. [PubMed: 18792069]

Zhong W, Chia W. Neurogenesis and asymmetric cell division. Curr Opin Neurobiol. 2008; 18:4–11. [PubMed: 18513950]

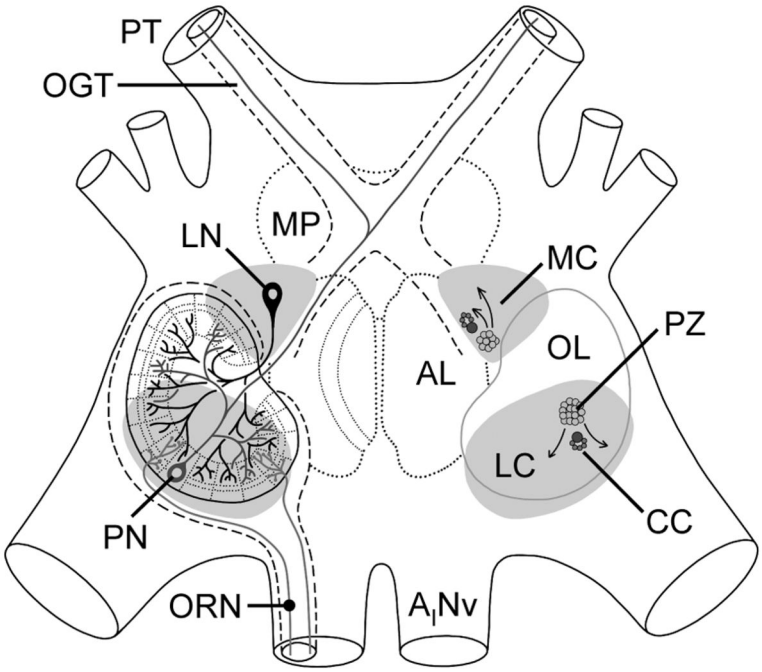

Figure 1.

Schematic representation of the organization of the olfactory deutocerebrum of the spiny lobster *P. argus* with respect to the location of neurogenic complexes. **Left:** Three primary types of neurons in the olfactory deutocerebrum: ascending projection neurons (PN) in gray, local interneurons (LN) in black, and olfactory receptor neurons (ORN) in light gray. **Right:** Location of proliferation zones (PZ) and associated clumps of cells (CC) in the lateral (LC) and medial (MC) soma clusters. Arrows indicate direction of movement of postmitotic cells generated in the proliferation zones. AL, accessory lobe; A_INv, antennular nerve; MP, medial protocerebrum; OGT, olfactory globular tract; OL, olfactory lobe; PT, protocerebral tract.

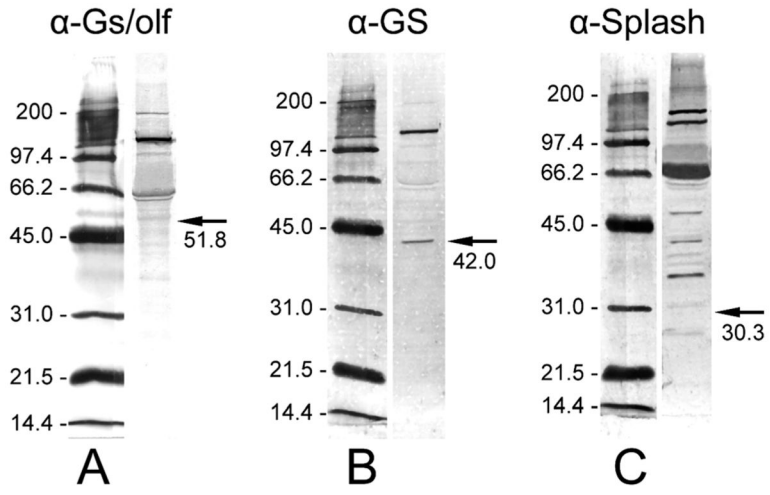

Figure 2.

Western blot analyses of total proteins extracted from *P. argus* brains with three antibodies used for the immunocytochemical characterization of the neurogenic complexes. **Left:** Alkaline-phosphatase-labeled molecular mass markers (indicated in kDa) visualized by NBT/BCIP running in the same SDS-PAGE gel as the antibody-labeled brain extract. **Right:** 10 μg *P. argus* brain extract labeled by one of the antibodies used for immunocytochemistry followed by detection through a secondary antibody labeled with alkaline phosphatase and its visualization by NBT/ BCIP. Arrows indicate the expected molecular mass (given below in kDa) of the target protein. **A:** Labeling with anti-Gs/olf revealed a double-band at an apparent molecular mass of ~61/63 kDa, a very prominent band at ~137 kDa, and a weak band at ~200 kDa. Gs cloned from the American lobster *H. americanus* has a molecular mass of ~51.8 kDa (Xu et al., 1997). **B:** Labeling with anti-GS revealed one band at the expected molecular mass of ~42 kDa that was reported for GS cloned from *P. argus* (Linser et al., 1997) and an additional very prominent band at ~136 kDa. **C:** Labeling with anti-Splash revealed at least six prominent bands at apparent molecular masses above the predicted molecular mass (30.3 kDa) of *P. argus* Splash (Chien et al., 2009).

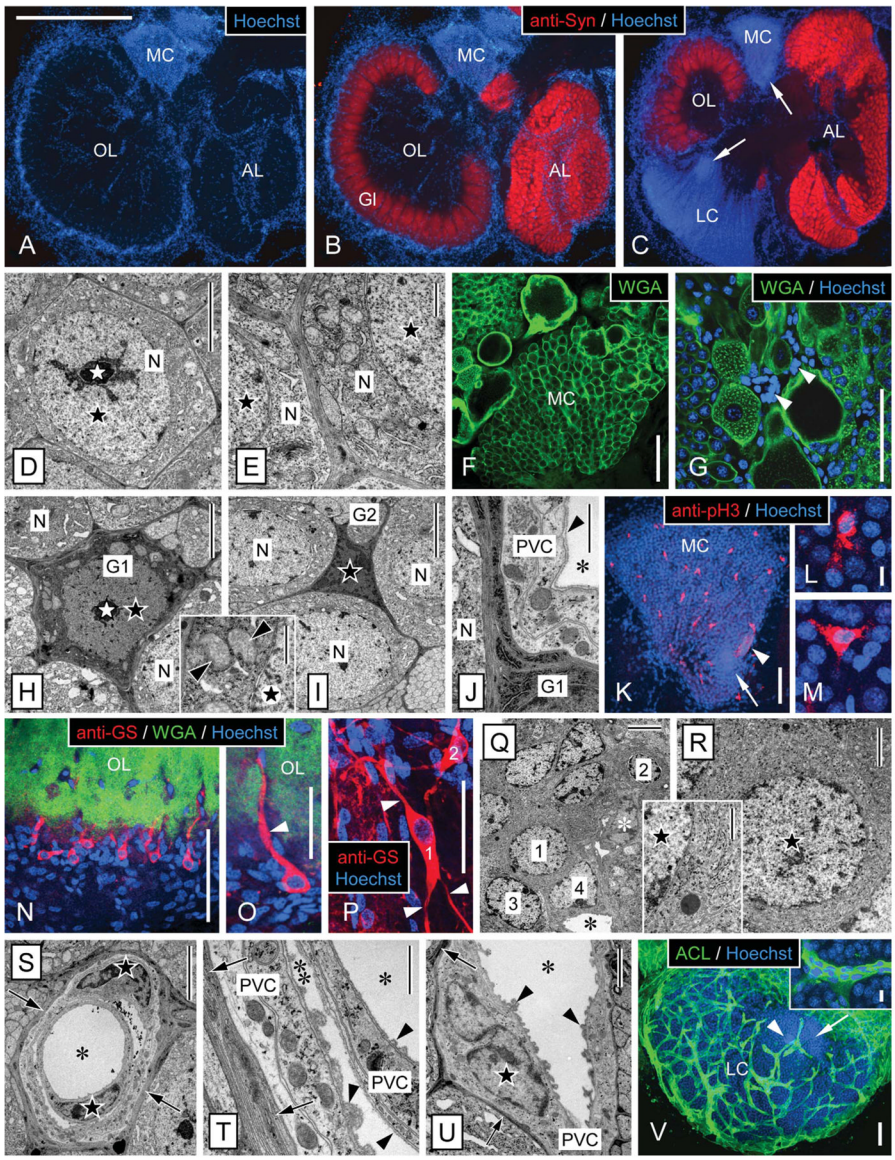

Figure 3.

Morphology of the olfactory deutocerebrum of *P. argus* and identification of its major cell types by TEM and selective markers. **A–C:** Main compartments of the olfactory deutocerebrum visualized by double labeling with anti-Syn and Hoechst 33258. Anti-Syn labeled synaptic areas within neuropils: the cortex of columnar glomeruli (Gl) of the olfactory lobe (OL) and the small spherical glomeruli of the accessory lobe (AL). Labeling with the nuclear marker Hoechst 33258 delineated the two large clusters of neuronal somata: the medial soma cluster (MC) and the lateral soma cluster (LC) and in addition numerous cells at the rim and in the center of the OL and AL. A,B: Horizontal section through the central aspect of the olfactory deutocerebrum with the OL at its largest extension. C: Horizontal section through the ventral aspect of the olfactory deutocerebrum with the AL at its largest extension. Within the LC and MC, the proliferation zones (arrows) located at the interior surface of the respective soma cluster can be distinguished based on their higher nuclear density. **D–G:** Identification of neurons by TEM and labeling with WGA. D: Soma of mature neuron (N) in the LC. The soma has a regular, slightly polyhedral shape and

contains an almost spherical nucleus (black star) with a centrally located nucleolus (white star). E: Cytoplasm of neuronal somata (N). A thick layer of cytoplasm surrounds the nucleus (black stars), and it contains numerous mitochondria and open ER cisternae as well as some Golgi apparatuses. F,G: Distribution of WGA labeling in the MC. F: In all neuronal somata, the cell membrane is distinctly labeled, and, in some large neuronal somata, the cytoplasm is also labeled in a punctate pattern. G: Double labeling with WGA and Hoechst 33258 revealed that numerous WGA^- cells (arrowheads) most likely representing glial cells and perivascular cells surround large WGA^+ neuronal somata. This labeling pattern establishes WGA as neuron-selective marker. **H–M:** Identification of cell body glia by TEM and labeling with anti-pH3. H: Type 1 cell body glia. The soma is relatively large (in the same size range as neuronal somata) and has an astrocyte-like, multipolar shape because of several processes extending between adjacent neuronal somata (N). It contains a thick layer of cytoplasm with numerous mitochondria (inset, arrowheads) surrounding a regularly shaped nucleus (black star) with a central nucleolus (white star). Cyto- and nucleoplasm are distinctly more electron dense than in neuronal somata. I: Type 2 cell body glia. The soma is small, of irregular shape, and almost completely filled by the irregularly shaped nucleus (black star). As in type 1 cell body glia, the soma extends several processes between adjacent neuronal somata (N) and cyto- and nucleoplasm are electron dense. J: Processes of cell body glia (G1) are characterized by electron-dense cytoplasm containing very electron-dense and robust cisternae of rough ER. Several layers of processes separate a neuronal soma (N) from perivascular cell processes (PVC) forming the wall of an adjacent arteriole (asterisk, lumen of arteriole; arrowhead, basal lamina). K–M: Double labeling with anti-pH3 and Hoechst 33258 in the medial soma cluster (MC). Anti-pH3 selectively labeled cells that based on size, distribution, and multipolar morphology (L,M) are identified as cell body glia (arrow, proliferation zone; arrowhead, clump of cells). **N–R:** Identification of type 1 neuropil glia by labeling with anti-GS and correlative TEM. N,O: Triple labeling with anti-GS, WGA, and Hoechst 33258 revealed a population of type 1 neuropil glia at the edge of the olfactory lobe (OL). Most of these cells are unipolar and extend one major process (arrowhead) into the WGA^+ OL neuropil usually running along a WGA^- arteriole. Note that GS^+ type 1 neuropil glia represent only a small fraction of the cells located at the edge of the OL neuropil whose nuclei are visualized by Hoechst 33258. P: Double labeling with anti-GS and Hoechst 33258 revealed multipolar (arrowheads) type 1 neuropil glia (1, 2) at the edge of the median protocerebral neuropil. Q: TEM revealed that the cell layer surrounding the OL neuropil is composed of diverse types of putative glial cells (1, 2, 3, 4) that among each other differ distinctly in nuclear morphology and/or cytoplasmic composition (white asterisk, nucleus of perivascular cell; black asterisk, lumen of arteriole). R: Putative glial cell at the edge of the OL neuropil (1 in Q) that corresponds to GS^+ type 1 neuropil glia in having an almost spherical nucleus, a thick layer of cytoplasm (inset: note delicate cisternae of rough ER), and unipolar morphology. **S–V:** Identification of perivascular cells by TEM and labeling with ACL. S–U: By TEM, arterioles are unequivocally identified as extracellular empty spaces representing the arteriole lumen (asterisks) enclosed by processes of perivascular cells (PVC) that are electron lucent and have a distinct cytoplasmic composition. The nuclei of perivascular cells (black stars) have an irregular, flattened shape and contain peripheral heterochromatin. Most arterioles are simple vessels (U), but some are complex, being composed of a vessel within a vessel (S,T), creating an inner (single asterisk) and an outer arteriole lumen (double asterisk). A basal lamina (arrowheads) composed of unstructured, flocculent material overlays all luminal surfaces of perivascular cell processes. Note that perivascular cells are separated from other tissue elements by an electron-dense layer (arrows) composed of processes of cell body glia. V: Double labeling with ACL and Hoechst 33258 revealed that, in the lateral soma cluster (LC), ACL intensely labels the net-like system of arterioles. Note that the proliferation zone (arrow) is less permeated by arterioles than the periphery of the LC and that the clump of cells (arrowhead)

is attached to an arteriole. Inset: Intense and uniform ACL labeling distinguishes perivascular cells from surrounding neuronal somata. Scale bar = 1 mm in A (applies to A–C); 5 μm in D,H,I,Q,S; 1 μm in E,J,T, H inset, Q inset; 100 μm in F,G,K,N,O,V; 10 μm in L (applies to L,M); 10 μm in V inset; 50 μm in P; 2 μm in R,U.

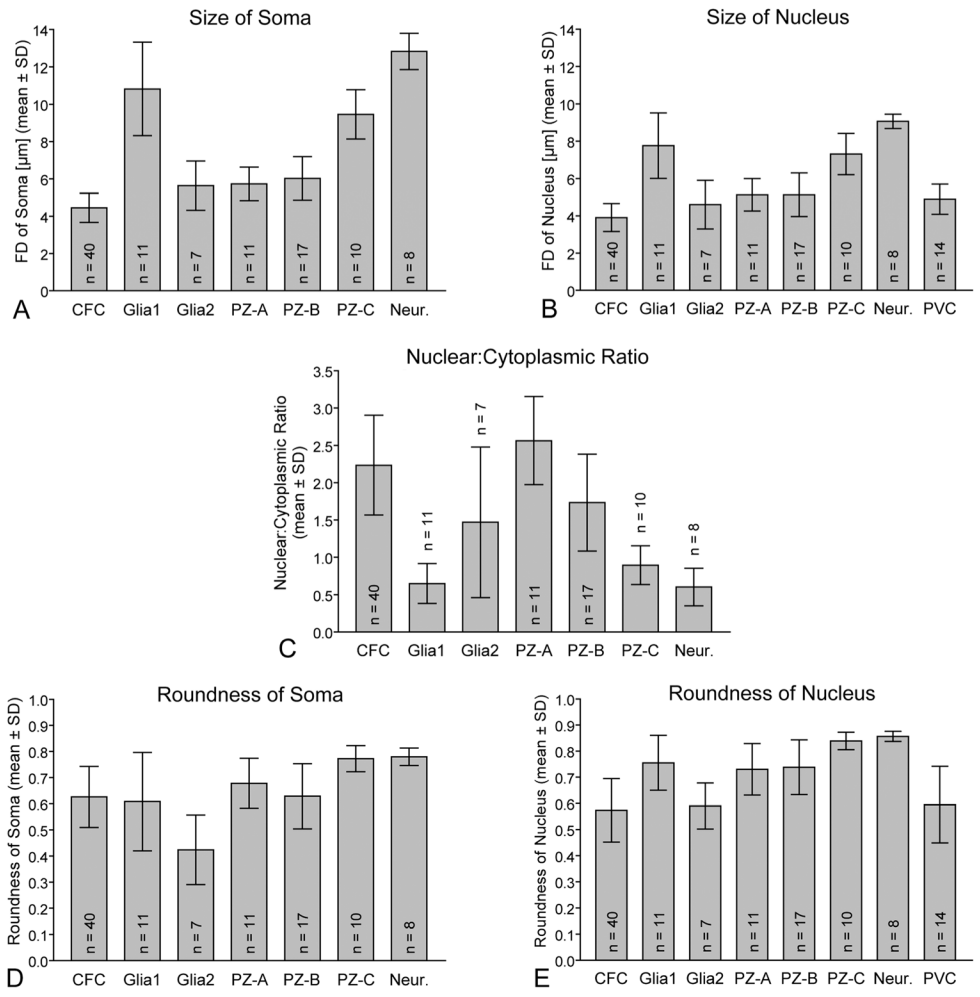

Figure 4.

Comparison of the main cell types present in the olfactory deutocerebrum of *P. argus* by quantification of the size and shape of their somata (**A,D**) and nuclei (**B,E**) and of their nuclear:cytoplasmic ratio (**C**) based on TEM micrographs. Size was measured as Feret diameter, shape was measured as roundness, and nuclear:cytoplasmic ratio was calculated by division of the nuclear volume by the cytoplasmic volume. Size and shape of somata as well as nuclear:cytoplasmic ratios were determined for seven cell types: clump-forming cells (CFC), type 1 cell body glia (Glia1), type 2 cell body glia (Glia2), type A proliferation zone cells (PZ-A), type B proliferation zone cells (PZ-B), type C proliferation zone cells (PZ-C), and neurons (Neur.). Size and shape of nuclei were determined for these seven cell types and in addition for perivascular cells (PVC). (PVCs are flat, sheath-like cells without clearly delimited soma and thus soma size and roundness could not be determined for them.) Numbers of measured cells are given as *n* in each column. Analysis of variance (ANOVA) showed statistically significant differences between the columns in each set of data ($P < 0.0001$); subsequent pairwise comparisons by Tukey's post hoc tests yielded significant differences between many data pairs. CFCs differed significantly ($P < 0.05$) from all other types of cells except type 2 cell body glia in soma and nucleus size. They also differed significantly from the other types of cells except type A and type B proliferation zone cells in nuclear:cytoplasmic ratio ($P < 0.05$). Thus, CFCs stand out from the other cell types in the olfactory deuto-cerebrum in being the smallest cells (Feret diameter of somata 4.4 ± 0.8 µm;

Feret diameter of nuclei 3.9 ± 0.7 μm) and in having a very high nuclear:cytoplasmic ratio (2.2 ± 0.7).

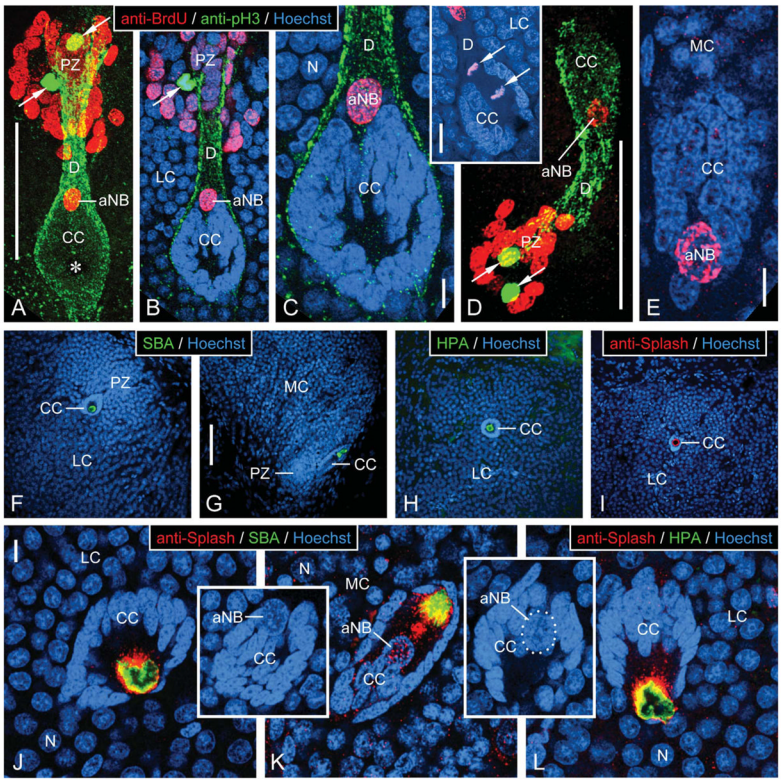

Figure 5.

Characterization of neurogenic complexes in the lateral and medial soma cluster by fluorescent labeling. **A–E:** Triple labeling with anti-BrdU, anti-pH3, and Hoechst 33258 after a single BrdU injection in the morning and 6 hours of survival time. **Inset:** Double labeling with anti-BrdU and Hoechst 33258. Micrographs represent collapsed stacks or substacks of optical sections (thickness 0.3–1.5 μm) from 80-μm-thick sections taken with a two-photon confocal microscope at three excitation wavelengths to visualize anti-BrdU (red), anti-pH3 (green), and Hoechst 33258 (blue). A–C: Lateral soma cluster (LC). D,E: Medial soma cluster (MC). A,D: Micrographs representing the entire section thickness omitting the Hoechst-33258 channel for clarity. A dense group of small $BrdU^+$ nuclei occupies the proliferation zone (PZ). Few $pH3^+$ nuclei (arrows) are located within the group of $BrdU^+$ nuclei. The proliferation zone is connected by a duct whose outer layer consists of fibrous $pH3^+$ material (D) to the clump of cells (CC), which at its PZ-facing pole contains the large $BrdU^+$ nucleus of an adult neuroblast (aNB). Note a nucleus- and label-free hole in the center of the clump of cells (asterisk in A) representing the bulbous foot of the aNB. B,C,E: Micrographs representing collapsed stacks of two (B), three (C, inset), or five (E) optical sections with a total thickness of 0.7 μm (B), 0.9 μm (C, inset), or 1.5 μm (E). The clump of cells (CC) consists of a cortex of small and densely packed nuclei of clump-forming cells that differ distinctly in size and shape from the $BrdU^+$ nucleus of the adult neuroblast (aNB) and from the nuclei of mature or maturing neurons (N). B,C: The clump of cells is surrounded by a layer of $pH3^+$ fibrous material that is contiguous with the material forming the outer layer of the duct (D) connecting with the proliferation zone (PZ). Note that a $pH3^+$ nucleus in the proliferation zone (arrow in B) is not $BrdU^+$, indicating that it was not in S-phase when BrdU was present. Inset: aNB captured in telophase of mitosis. Note that the mitotic plane is perpendicular to the long axis of the clump of cells and duct; condensed daughter nuclei (arrows). **F–L:** Labeling with lectins and anti-Splash demonstrating that the bulbous foot of the adult neuroblast is immunocytochemically

privileged. Micrographs represent collapsed stacks or substacks of optical sections (thickness 0.3–1.5 μm) from 80-μm-thick sections taken with a two-photon confocal microscope at two or three excitation wavelengths to visualize Hoechst 33258 (blue) and anti-Splash (red), SBA (green), or HPA (green). F–I: Micrographs at low magnification demonstrate that in the lateral soma cluster (LC; F,H,I) and in the medial soma cluster (MC; G), SBA (F,G), HPA (H), and anti-Splash (I) selectively label the center of the clump of cells (CC) containing the bulbous foot of the adult neuroblast. J–L: Micrographs at higher magnification reveal that the lectin^{+} area in the nucleus-free center of the clump of cells (CC) is surrounded by Splash^{+} material. Note that the large nucleus of the adult neuroblast (aNB; in insets on different optical sections with the same orientation as in J and L; in inset K, nucleus of adult neuroblast outlined by white dots) is located at the pole of the clump of cells opposing the nucleus-free center. Scale bars = 100 μm in A (applies to A,B); 10 μm in C,E; 20 μm in C inset; 100 μm in D; 100 μm in G (applies to F–I); 10 μm in J (applies to J–L, J,K insets).

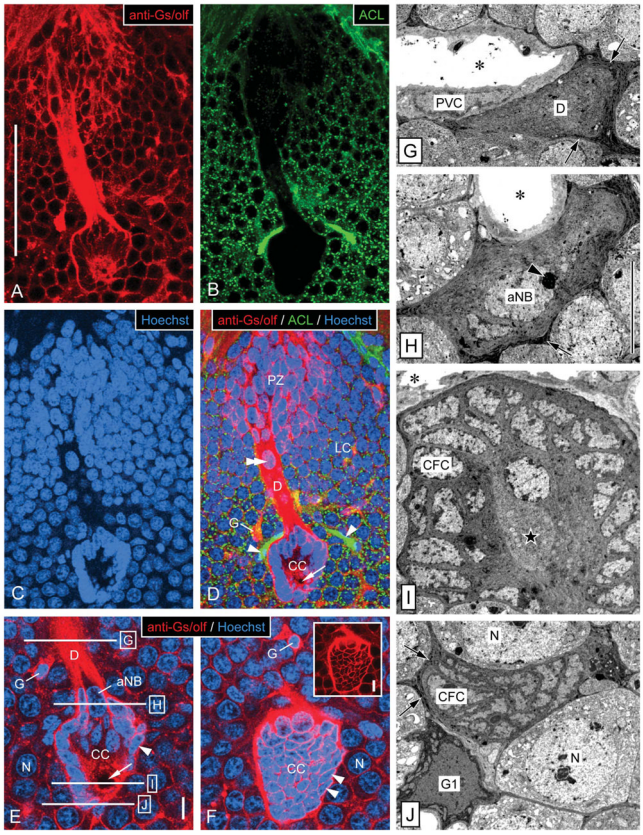

Figure 6.

Overview of ultrastructure of the neurogenic complex in the lateral soma cluster by correlation of fluorescent labeling and TEM. **A–F:** Fluorescent labeling of a sagittal vibrating-microtome section through the neurogenic complex in the lateral soma cluster (LC) with anti-Gs/olf (red in A,D–F), ACL (green in B,D), and Hoechst 33258 (blue in C–F). Micrographs represent collapsed stacks of eight (A–D) or three (E,F) optical sections with a total thickness of 5.6 μm (A–D) or 0.9 μm (E, F). A–D: Low magnification reveals the spatial correlation of the three main components of the neurogenic complex: proliferation zone (PZ), clump of cells (CC), and duct (D) connecting them. The neurogenic complex stands out from the neuronal somata in its surround by being more intensely labeled by anti-Gs/olf (A), by being ACL^{-} (B), and by having a unique arrangement of cell nuclei (C). Note that ACL intensely labels arterioles (asterisks) one of which is attached to the clump of cells, that anti-Gs/olf also intensely labels cell body glia (G), that the nucleus-free center of the clump of cells contains a round area devoid of Gs/olf-like immunoreactivity (arrow), and that the duct contains a large oval nucleus (double arrowhead). E,F: Higher magnification reveals the organization of the clump of cells (CC) at two levels of one stack of optical sections. E: Section through the midplane of the clump of cells. Small nuclei of clump-forming cells (arrowhead) form a dense cortex around a nucleus-free center that contains a round area that is Gs/olf^{-} (arrow). At the origin of the duct (D), the clump-forming cells (CFC) surround the large oval nucleus of the adult neuroblast (aNB). A cell body glial cell (G) has a denser nucleus than surrounding neurons (N), and one of its Gs/olf^{+} processes connects with the duct. Approximate levels of TEM cross-sections through the duct and clump of cells (G,H) indicated by horizontal lines. F: Section through the cortex of the clump of cells. The cortex of the clump of cells is formed by closely associated somata of clump-forming cells (arrowheads) that have very little

cytoplasm (inset: Hoechst signal omitted for clarity) surrounding their dense nucleus. The clump of cells is surrounded by neuronal somata (N) and interspersed Gs/olf$^+$ cell body glia (G). **G–J:** Low-magnification TEM micrographs of cross-sections through the duct and the clump of cells in the lateral soma cluster at levels indicated in E. G: Cross-section through the duct. The duct (D) is a massive strand of tissue composed of the distal processes of clump-forming cells and is surrounded by a layer of electron-dense processes of cell body glia (arrows). A large arteriole whose lumen (asterisk) is surrounded by processes of perivascular cells (PVC) is attached to the duct. H: Cross-section through the apex of the clump of cells. Processes of clump-forming cells (CFC) form a thick continuous layer around the peripheral domain of the adult neuroblast (aNB) characterized by a large nucleus with a large, peripheral nucleolus (arrowhead; arrows, layer of electron-dense processes of cell body glia surrounding the clump of cells; asterisk, lumen of attached arteriole). I: Cross-section through the center of the clump of cells. Somata of clump-forming cells (CFC) form a dense cortex around a nucleus free center filled by their inner processes and the bulbous foot of the adult neuroblast (star; asterisk, lumen of attached arteriole). J: Cross-section through the bottom of the clump of cells. The contiguous cortex of the clump of cells formed by somata of clump-forming cells (CFC) is surrounded by a layer of electron-dense processes of cell body glia (arrows) some of which are contributed by a type 1 cell body glia in the immediate vicinity (G1). N, neuronal soma. Scale bars 100 μm in A (applies to A–D); 10 μm in E (applies to E,F); 10 μm in inset; 10 μm in H (applies to G–J).

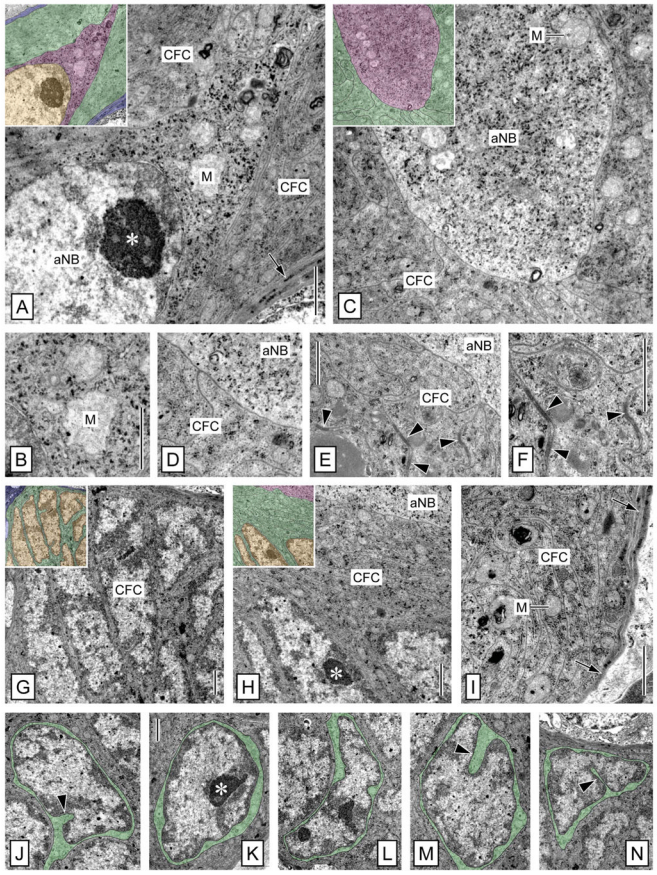

Figure 7.

Ultrastructure of the clump of cells: Clump-forming cells and adult neuroblast. TEM micrographs of cross-sections through the clump of cells in the lateral soma cluster. Colorized insets highlight different cell types: adult neuroblast (magenta), clump-forming cells (green), processes of cell body glia (blue), nuclei of all cell types (yellow). **A,B:** Peripheral domain of the adult neuroblast (aNB) at the apex of the clump of cells. The electron-lucent cytoplasm of the peripheral domain of the aNB contains large electron-lucent mitochondria (M) and numerous electron-dense granules. The peripheral domain of the aNB is completely covered by outer processes of clump-forming cells (CFC) whose cytoplasm differs distinctly from that of the aNB in electron density and organelle composition (arrow, processes of cell body glia; asterisk, nucleolus). **C–F:** Bulbous foot of the adult neuroblast (aNB) in the nucleus-free center of the clump of cells. The bulbous foot of the aNB is identical to the peripheral domain in having electron-lucent cytoplasm containing large electron-lucent mitochondria (M) and numerous electron-dense granules. The bulbous foot of the aNB is completely covered by the inner processes of clump-forming cells (CFC). No membrane specializations are apparent at the interface between aNB and CFCs. Occasional desmosome-like membrane specializations are present between adjacent processes of different CFCs (arrowheads). **G–N:** Ultrastructure of clump-forming cells (CFC). G: Cortex of the clump of cells. The cortex of the clump of cells is formed by a continuous layer of CFC somata characterized by a relatively large and irregularly shaped nucleus and only a thin rim of cytoplasm. H,I: Nucleus-free center of the clump of cells. The nucleus-free center of the clump of cells is filled by the bulbous foot of the aNB and a thick layer of inner processes of clump-forming cells (CFC) surrounding it. The cytoplasm of the CFC processes is of medium electron density and contains small mitochondria (M) and delicate cisternae of

rough ER (arrows, processes of cell body glia; asterisk, nucleolus). J–N: Somata of clump-forming cells with cytoplasm colorized green to highlight the irregular and diverse shape of somata and nuclei as well as the high nuclear:cytoplasmic ratio of CFCs. Note deep invaginations present in some CFC nuclei (arrowheads). Asterisk, nucleolus. Scale bars = 1 μm A (applies to A,B); 1 μm in B (applies to B,D); 1 μm in E–I; 1 μm in K (applies to J–N).

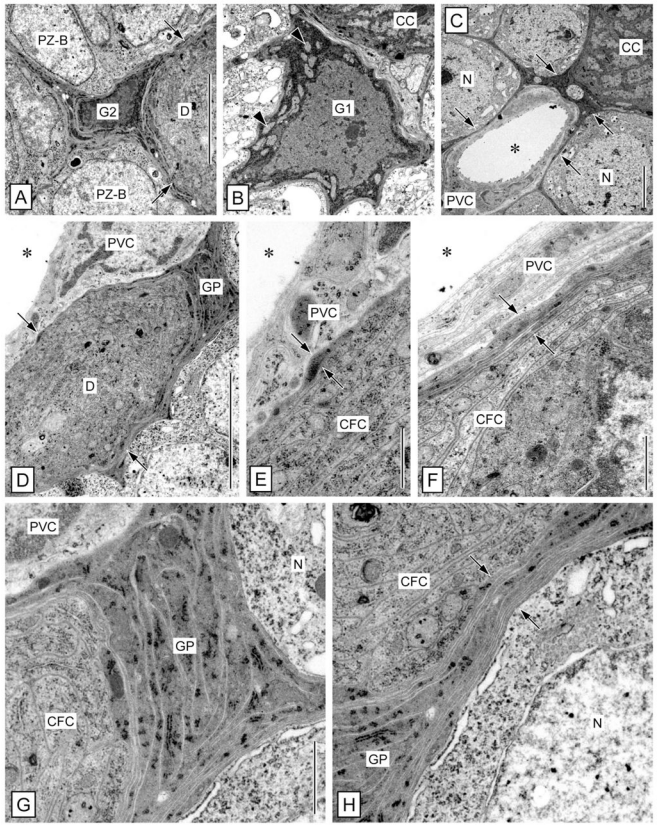

Figure 8.

Ultrastructure of the clump of cells and duct: glial sheath and association with arteriole. TEM micrographs of cross-sections through the duct or the clump of cells in the lateral soma cluster. **A:** Type 2 cell body glia (G2) closely associated with the duct (D). From the soma of the type 2 cell body glia, processes extend between surrounding type B proliferation zone cells (PZ-B) and contribute to the glial sheath surrounding the duct (arrows). **B:** Type 1 cell body glia (G1) closely associated with the clump of cells (CC). Note multipolar morphology of the soma and numerous electron-lucent mitochondria (arrowhead) in the electron-dense cytoplasm. **C:** Arteriole attached to the clump of cells. A simple arteriole with a lumen (asterisk) surrounded by a layer of processes of perivascular cells (PVC) is separated from neuronal somata (N) and from the clump of cells (CC) by a continuous layer of electron-dense processes of cell body glia (arrows). **D–F:** Separation of duct and clump of cells from the attached arteriole. D,E: The outer processes of clump-forming cells (CFC) that constitute the duct (D) are surrounded by a layer of electron-dense processes of cell body glia (GP; arrows). Only one process of cell body glia (opposing arrows in E) separates the CFC processes from the perivascular cell (PVC) surrounding the lumen of the attached arteriole (asterisk). F: At the clump of cells, several processes of cell body glia (opposing arrows) separate the clump-forming cells (CFC) from the perivascular cell processes (PVC) surrounding the lumen of the attached arteriole (asterisk). **G,H:** Separation of duct and clump of cells from neuronal somata. G: A thick accumulation of numerous processes of cell body glia (GP) is interspersed between the outer processes of clump-forming cells (CFC) forming the duct and adjacent neuronal somata (N). H: At the clump of cells, multiple processes of cell body glia (GP; opposing arrows) separate the clump-forming cells (CFC) from adjacent neuronal somata (N). Scale bars = 5 μm in A (applies to A,B); 5 μm in C,D; 1 μm in E,F; 1 μm in G (applies to G,H).

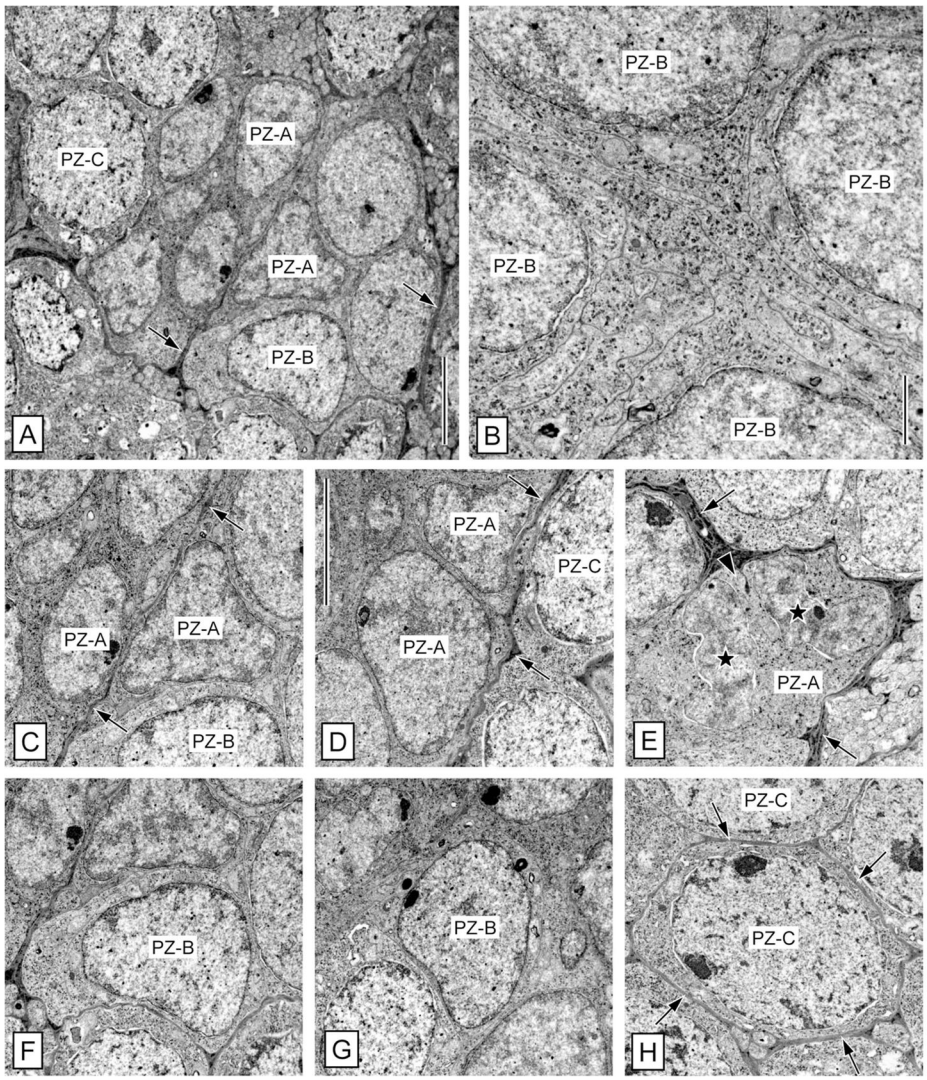

Figure 9.

Ultrastructure of the proliferation zone. TEM micrographs of sections through the proliferation zone in the lateral soma cluster. **A:** Center of proliferation zone at low magnification reveals the presence of three distinct cell types: type A (PZ-A), type B (PZ-B) and type C cells (PZ-C). Note that layers of electron-dense processes of cell body glia (arrows) only partially separate cells from each other. **B:** Four neighboring type B cells (PZ-B). Type B cells are not surrounded by processes of cell body glia. They form irregularly shaped, convoluted processes that interdigitate with processes of other type B cells. The inner nuclear membrane is distinctly thicker than the outer one. **C,D:** Two examples of type A cells (PZ-A) at higher magnification. Type A cells have an irregularly shaped nucleus with large areas of diffuse heterochromatin. Note the distinctly different appearance of type B (PZ-B) and type C (PZ-C) cells in the surround (arrows, layers of electron-dense processes of cell body glia). **E:** Type A cell (PZ-A) in telophase of mitosis. Condensed daughter nuclei (stars) oppose each other. Thin cell membranes separate the two daughter cells (arrowhead; arrows indicate layers of electron-dense processes of cell body glia). **F,G:** Two examples of type B cells (PZ-B). Type B cells have a thicker rim of cytoplasm and a more regularly shaped nucleus than type A cells. Their inner nuclear membrane is distinctly thicker and more electron dense than the outer one. **H:** Example of a type C cell. Type C

cells (PZ-C) are larger and have a more spherical nucleus than type A and type B cells. Note that a distinctive gap separates both nuclear membranes and that the cell is completely surrounded by a layer of electron-dense processes of cell body glia (arrows). Scale bars = 5 μm in A; 1 μm in B; 5 μm in D (applies to C–H).

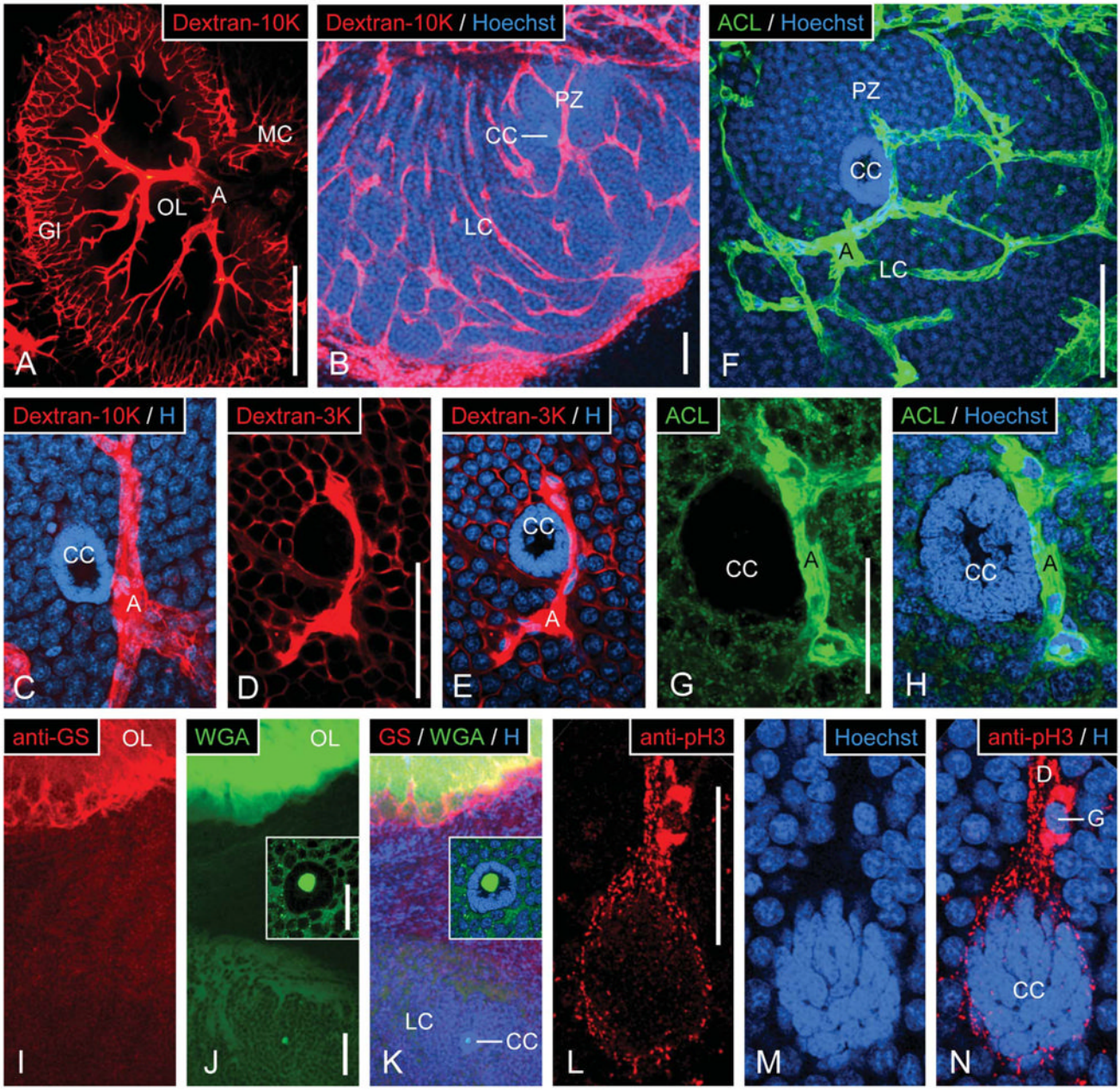

Figure 10.

Access of hemolymph to the clump of cells and its labeling with selective fluorescent markers. **A–E:** Single or double labeling in the olfactory deutocerebrum by fluorescent dextrans perfused into the cerebral artery and Hoechst 33258. A: Vascularization of the olfactory lobe; micrograph represents an epifluorescent image of the dextran-tetramethylrhodamine signal captured by a CCD camera. A large arteriole (A) penetrates the olfactory lobe (OL) via the anterior foramen and develops tree-like branches in the OL core. These branches give rise to a very dense net of fine arterioles in the glomerular cortex (Gl). Some side branches project into the medial soma cluster (MC). B–E: Micrographs represent collapsed substacks of optical sections (thickness 0.3–1.5 μm) from 80-μm-thick sections taken with a two-photon confocal microscope at two excitation wavelengths to visualize dextran-tetramethylrhodamine (red) and Hoechst 33258 (blue). B: Vascularization of the

lateral soma cluster. The lateral soma cluster (LC) is permeated by a net-like system of arterioles only one of which crosses through the proliferation zone (PZ). The clump of cells (CC) is attached to this arteriole. C: Clump of cells in the lateral soma cluster after perfusion of 10,000-MW dextran into the cerebral artery. The clump of cells (CC) is attached to an intensely dextran^{+} arteriole (A) but is itself totally devoid of dextran labeling. D: Clump of cells in the lateral soma cluster after perfusion of 3,000-MW dextran into the cerebral artery. The clump of cells (CC) is totally devoid of dextran labeling, whereas the arteriole (A) attached to it and spaces between neuronal somata are dextran^{+}. **F–H:** Double labeling with ACL and Hoechst 33258 in the lateral soma cluster. Micrographs represent collapsed substacks of optical sections (thickness 0.3–1.5 μm) from 80-μm-thick sections taken with a two-photon confocal microscope at two excitation wavelengths to visualize ACL-FITC (green) and Hoechst 33258 (blue). In the lateral soma cluster (LC), ACL intensely labels a net-like system of arterioles (A) and particles within the cytoplasm of neuronal somata. The clump of cells (CC) is attached to an arteriole (A) but is itself completely devoid of ACL labeling. **I–K:** Triple labeling with anti-GS, WGA, and Hoechst 33258 in the olfactory lobe and the lateral soma cluster. Micrographs represent collapsed substacks of optical sections (thickness 0.3–1.5 μm) from 80-μm-thick sections taken with a two-photon confocal microscope at three excitation wavelengths to visualize anti-GS (red), WGA-AlexaFluor488 (green) and Hoechst 33258 (blue). Neuropil glia at the edge of the WGA^{+} olfactory lobe (OL) are intensely GS^{+} but the WGA^{+} lateral soma cluster (LC) including the clump of cells (CC) is completely devoid of GS labeling. **Insets:** Clump of cells at higher magnification. **L–N:** Double labeling with anti-pH3 and Hoechst 33258 in the lateral soma cluster. Micrographs represent collapsed substacks of optical sections (thickness 0.3–1.5 μm) from 80-μm-thick sections taken with a two-photon confocal microscope at two excitation wavelengths to visualize anti-pH3 (red) and Hoechst 33258 (blue). Cell body glia (G) and the glial sheath of fibrous material surrounding the clump of cells (CC) and the duct (D) are intensely pH3^{+}, whereas the clump-forming cells are pH3^{-}. Scale bars = 500 μm in A; 100 μm B; 100 μm in D (applies to C–E); 100 μm in F; 50 μm in G (applies to G,H); 100 μm in J (applies to I–K); 50 μm in J inset (applies to J inset, K inset); 50 μm in L (applies to L–N).

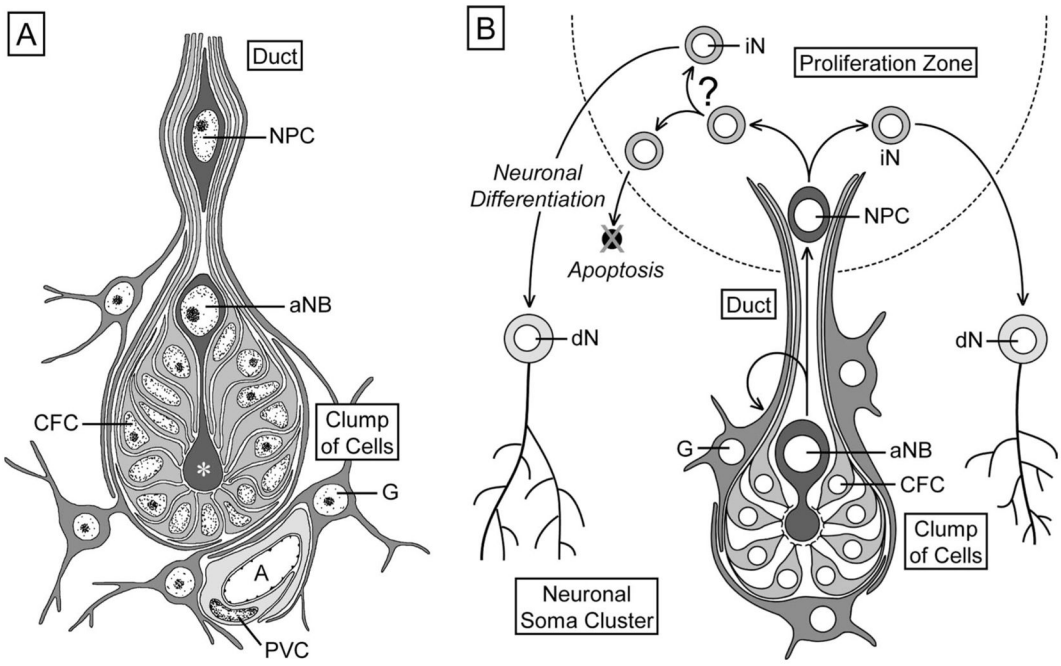

Figure 11.

A: Schematic representation of the cytoarchitecture of the clump of cells in the lateral soma cluster of *P. argus*. The clump of cells is composed of bipolar clump-forming cells (CFC) whose somata form a continuous cortex around a nucleus-free center. One process of the clump-forming cells is short and faces inward; the other one is long and faces outward. Together, the outward-facing processes form the duct connecting with the adjacent proliferation zone. The clump-forming cells completely enclose one adult neuroblast (aNB), which consists of two large domains connected by a thin bridge and thus has an hourglass-like shape. The peripheral domain of the adult neuroblast contains the nucleus and is located at the apical pole of the clump of cells. The other domain forms a bulbous foot (asterisk) within the nucleus-free center of the clump of cells and is surrounded by the inner processes of CFCs. The clump of cells and the duct are surrounded by a continuous layer of processes of multipolar cell body glia (G). The clump of cells is associated with an arteriole (A) whose wall is constituted by processes of perivascular cells (PVC). The duct contains elongated cells that most likely represent neuronal progenitor cells (NPC) that are produced by asymmetric divisions of the aNB and migrate through the duct to the adjacent proliferation zone. **B:** Schematic representation of the current model of cell divisions and lineages maintaining adult neurogenesis in the olfactory deutocerebrum of *P. argus*. In each neuronal soma cluster of the olfactory deutocerebrum, production of new neurons is based on one neural stem cell, which is an adult neuroblast (aNB) located close to the proliferation zone and embedded in a clump of cells. Through serial asymmetric divisions, the aNB renews itself and produces differentiating daughter cells at its apical pole. Within a duct formed by processes of the clump-forming cells (CFC), the daughter cells migrate to the proliferation zone, where they replenish the pool of neuronal progenitor cells (NPCs). Ultimately, neuronal progenitor cells divide once symmetrically and produce two daughter cells that represent immature neurons (iN). Migrating out of the proliferation zone, most of the immature neurons become differentiated neurons (dN) within months, but some die by apoptosis. We propose that, upon their arrival in the proliferation zone, daughter cells generated by the aNB may undergo one or more fast rounds of cell divisions and thus represent transit amplifying intermediate progenitor cells, accommodating the continuous replenishment of 30 (MC) or 100 (LC) cells in S-phase in the proliferation zone by only one

aNB. For adult *P. argus*, there is no evidence for proliferation of the CFCs or the cell body glia (G) surrounding the clump of cells, making it unlikely that these two cell types contribute to maintaining adult neurogenesis.

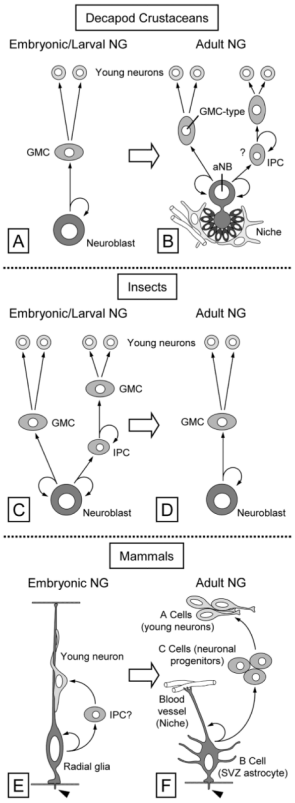

Figure 12.

Schematic comparison of neural stem cells and cell lineages maintaining embryonic/larval and adult neurogenesis in the brain of decapod crustaceans (**A,B**), insects (**C,D**), and mammals (**E,F**). A: Embryonic and larval neurogenesis in crustaceans is based on large, spherical neuroblasts, which through a series of asymmetric divisions self-renew and generate ganglion mother cells (GMC) into the interior of the body. Each GMC divides symmetrically once and generates two immature neurons. B: Adult neurogenesis in decapod crustaceans is maintained by large, hourglass-shaped adult neuroblasts (aNB), which are closely associated with a stem cell niche composed of clump-forming cells, glial cells, and an attached arteriole. Through a series of asymmetric divisions the aNB self-renews and ultimately gives rise to GMC-type neuronal progenitor cells, each of which divides symmetrically once and generates two immature neurons (left lineage). We hypothesize that the daughter cells produced by the aNB divisions likely act as transient-amplifying intermediate progenitor cells (IPC), each of which produces multiple GMC-type neuronal progenitors (right lineage). C: Embryonic and larval neurogenesis in insects is mostly as in crustaceans and is based on “canonical” neuroblasts (left lineage). Some embryonic and larval neuroblast lineages contain transit-amplifying intermediate progenitor cells (IPC) that through asymmetric divisions self-renew and generate GMCs (right lineage; modified from Bello et al., 2008). D: Adult neurogenesis in insects appears to be maintained by “canonical” neuroblasts and their embryo-typical lineage. E: In embryonic neurogenesis of mammals, radial glial cells serve as neural stem cells. Through asymmetric divisions they self-renew and ultimately generate daughter cells that, after migrating along the radial glial process, mature into neurons. The generation of neurons could be direct or through transit-amplifying intermediate progenitor cells (IPC?). One hallmark feature of radial glia cells is to have a primary cilium reaching into the ventricle (arrowhead). Modified from Alvarez-Buylla et al. (2001). F: Adult neurogenesis in the SVZ of mammals is maintained by type B cells, which

have an astrocytic morphology and possess a primary cilium (arrowhead) reaching into the ventricle. Type B cells are slowly cycling neural stem cells, which through asymmetric divisions self-renew and generate rapidly dividing neuronal progenitor cells (C cells). C cells give rise to immature neurons (A cells). Type B cells are associated with morphologically complex stem cell niches, one element of which are blood vessels directly contacted by type B cell processes. Modified from Kriegstein and Alvarez-Buylla (2009).

TABLE 1

Primary Antibodies

Abbreviation	Antigen	Host	Supplier/reference	Catalog No.	Dilution
Anti-BrdU	5-Iodo-2′-deoxyuridine	Mouse monoclonal	Becton Dickinson Biosciences	B44	1:150
Anti-pH3	Amino acids 7–20 (ARK[pS]TGGKAPRKQLC) of human histone H3	Rabbit polyclonal	Upstate Biotechnology	06–570	1:250
Anti-Syn	sSmall isoform of synapsin (SYNAORF-1) of *Drosophila*	Mouse monoclonal	Developmental Studies Hybridoma Bank; Klagges et al., 1996	3C11	1:25
Anti-Gs/olf	amino acids 377–394 of Gas of rat	Rabbit polyclonal	Santa Cruz Biotechnology	sc-383	1:200
Anti-GS	Amino acids 1–373 of sheep glutamine synthetase	Mouse monoclonal	Becton Dickinson Biosciences	610518	1:100
Anti-Splash	Amino acids 133–265 of spiny lobster *achaete scute* homolog	Rabbit polyclonal	Dr. Hsin Chien (GSU); Chien et al., 2009		1:400